

Design of a Mars Rover Suspension Mechanism

By
Firat Barlas

**A Dissertation Submitted to the
Graduate School in Partial Fulfillment of the
Requirements for the Degree of**

MASTER OF SCIENCE

**Department: Mechanical Engineering
Major: Mechanical Engineering**

**Izmir Institute of Technology
Izmir, Turkey**

June, 2004

We approve the thesis of **Fırat Barlas**

Date of Signature

15.06.2004

Prof. Dr. Tech. Sc. Rasim ALİZADE

Supervisor

Department of Mechanical Engineering

15.06.2004

Asst. Prof.Dr. Serhan ÖZDEMİR

Department of Mechanical Engineering

15.06.2004

Prof.Dr. Refail ALİZADE

Department of Mathematics

15.06.2004

Assoc.Prof.Dr. Barış ÖZERDEM

Head of Mechanical Engineering Department

ACKNOWLEDGMENT

Space and engineering have been the biggest passion of mine since my childhood. The solar system exploration is a dream of everyone including me. In this thesis study, I had a chance to combine these things into a scientific work. During my research phase, it was amazing to work and discuss with the eminent scientist, the kind person Professor Rasim Alizade who helped me with his wide knowledge and experience in kinematics. I would like to thank him deeply for his wonderful contribution to this study.

There are also many friends who shared their precious ideas in Izmir Institute of Technology and forced me to complete this work. I wish to thank Özgür Kilit who helped me with his different approach to kinematics problems and solution methods.

Last of all, I am thankful to my dear family for their never-ending support and belief in me. This work could not have been done without them.

Fırat Barlas
İzmir – June 2004

“In order to understand the universe, it is necessary to understand the language in which its laws are written and that language is mathematics”

Galilei Galileo (1564-1642)

ABSTRACT

It is obvious that rovers are important vehicles of today's solar system exploration. Most of the rover designs have been developed for Mars and Moon surface in order to understand the geological history of the soil and rocks. Exploration operations need high speed and long distance traversal in a short mission period due to environmental effects, climate and communication restrictions. Several mechanisms have been suggested in recent years for suspensions of rovers on rough terrain. Although their different mechanisms have found a widespread usage in mobile robotics, their low operation speed is still a challenging problem. In this research, a new suspension mechanism has been designed and its kinematic analysis results were discussed. Standard rocker-bogie suspension mechanism, which has been developed in the late 1990's, has excellent weight distribution for different positions on rough terrain. New design, mostly similar to rocker-bogie suspension system, has a natural advantage with linear bogie motion which protects the whole system from getting rollover during high speed operations. This improvement increases the reliability of structure on field operations and also enables the higher speed exploration with same obstacle height capacity as rocker-bogie.

In this thesis study, new bogie mechanism consisted of double-lambda mechanisms, which has been firstly presented by Pafnuty Lvovich Chebyshev in 1869, is solved by analytically to define the positions and singular configurations. A new structural synthesis formula also has been introduced for such suspension mechanisms with lower and higher kinematic pairs. By using structural synthesis methods, a suspension mechanism has been designed with double-lambda mechanism. Equivalent force and moment functions were also derived with equation of motion method.

The results are confirmed with the computer analysis made by Visual Nastran 4D[®]. For this purpose, a computer model has been constructed and assembled with the same design parameters of NASA Mars Exploration Rovers (MER1 and MER2).

ÖZ

Hiç şüphesiz günümüz güneş sistemi keşif araçlarından en önemlileri gezer robotlarıdır. Ay ve Mars yüzeyindeki kum ve taşların jeolojik yapısını anlamak amacıyla pek çok robot tasarımı geliştirilmiştir. Kısıtlı görev süresi, çevresel etkiler, iklim ve iletişim kısıtları nedeniyle keşiflerin yüksek hız ve uzun mesafeler kat ederek yapılmasına ihtiyaç duyulmaktadır. Geçtiğimiz yıllar boyunca, bozuk yüzey üzerinde çalışan gezer robotlar için birçok süspansiyon mekanizması önerilmiştir. Mobil robotlar üzerinde geniş kullanım alanı bulmalarına karşın bu mekanizmaların düşük hızları hala ciddi problem oluşturmaktadır. Bu araştırmada yeni bir süspansiyon mekanizması tasarlanmış ve kinematik analizi tartışılmıştır. 1990'lı yılların başında geliştirilen “rocker-bogie”, değişik pozisyonlarda mükemmel ağırlık dağıtma özelliğine sahiptir. Genel olarak “rocker-bogie” mekanizmasına benzer olan yeni tasarım sahip olduğu doğrusal hareketli “bogie” bileşeni ile yüksek sürat ile hareket sırasında takla atmaya engelleyici doğal bir üstünlüğe sahiptir. Bu geliştirme, yüzey operasyonları sırasında sistemin güvenilirliğini artırmakta, hem de “rocker-bogie” süspansiyonu ile aynı engel aşma kapasitesine sahip olmasının yanında yüksek hızda keşfe olanak sağlamaktadır.

Bu tez çalışmasında ilk olarak Pafnuty Lvovich Chebyshev'in 1869 yılında sunduğu lamda mekanizmasının çift olarak birleştirilmesi ile elde edilen “bogie” mekanizmasının analitik olarak pozisyon ve ölü durum analizleri yapılmıştır. Aynı zamanda adi ve yüksek eleman çiftleri için yeni bir yapısal sentez formülü geliştirilmiştir. Yapısal sentez metodları kullanılarak çift lamda mekanizması ile yeni bir süspansiyon mekanizması geliştirilmiştir. Hareket denklemi yöntemi ile eşdeğer kuvvet ve moment fonksiyonları da elde edilmiştir.

Sonuçlar Visual Nastran 4D[®] ile yapılan bilgisayar analizleri ile doğrulanmıştır. Bu amaçla NASA Mars Keşif Robotları (MER1 ve MER2) 'na ait tasarım parametrelerine uygun olarak bilgisayar modelleri oluşturulmuştur.

TABLE OF CONTENTS

LIST OF FIGURES	xi
Chapter 1 INTRODUCTION.....	1
1.1 Mobile Robots and Description of “Rover”	2
1.1.1 Definition of Mobile Robot	2
1.1.2 Locomotion	3
1.2 History of Rovers	4
1.2.1 Lunakhod	4
1.2.2 Sojourner	4
1.2.3 Inflatable Rover	5
1.2.4 Rocky 7	6
1.2.5 Sample Return Rover	7
1.2.6 Nanorover	7
1.2.7 Micro5	8
1.2.8 Shrimp	8
1.2.9 Mars Exploration Rovers (MER)	9
1.3 Rover Operations and Future Requirements	10
Chapter 2 WHEELED LOCOMOTION AND SUSPENSION	11
2.1 Suspension	11
2.2 Obstacle Capacity	12
2.3 Wheel Forces	13
2.4 Rocker-Bogie Suspension	14
2.5 Wheel Motion	15
2.6 Advantage of Linear Motion	16

Chapter 3	STRAIGHT LINE MECHANISMS	18
3.1	Chebyshev Mechanism	18
3.2	Watt's Linkage	19
3.3	Robert's Linkage	20
3.4	Chebyshev's Lambda Mechanism (Hoeken Mechanism)	21
Chapter 4	STRUCTURAL SYNTHESIS AND DESIGN OF SUSPENSION MECHANISM	23
4.1	Structural Synthesis	23
4.1.1	Mobility Analysis	23
4.1.2	Structural Synthesis Formula for Lower and Higher Kinematic Pairs	24
4.1.3	Structural Groups	26
4.1.4	Closed Chain Construction with Structural Groups	27
4.1.5	Structural Synthesis of Bogie Mechanism	29
4.2	Design	30
4.2.1	Design Parameters Selection	30
4.2.2	Geometric Trajectory of Lambda Mechanism	31
4.2.3	Singularity	32
4.2.3.1	First Singularity	33
4.2.3.2	Second Singularity	33
4.2.4	Double-Lambda Mechanism Connection	34
4.2.5	Adaptation of double-lambda mechanism into Rocker-Bogie suspension: LBS	35
4.2.6	Mobility Analysis of LBS Mechanism	36
4.2.7	Various design possibilities with linear bogie	37

Chapter 5 POSITION ANALYSIS OF LAMBDA MECHANISM	38
5.1 Coupler Curve Function and Trajectory of the Wheel	38
5.1.1 Vector Loop Equations	38
5.1.2 Angular Relations	40
5.1.3 Coupler Curve Function	41
5.2 Singularity Analysis	42
5.2.1 Singular Configurations Relative to α	42
5.2.2 Singular Configurations Relative to θ	44
5.3 Symmetric Side Inverse Position Analysis	46
5.4 Singular Positions of Double-Lambda Bogie Mechanism	48
Chapter 6 STATIC ANALYSIS	49
6.1 Wheel Reaction Forces	49
6.2 Stability Definition of a Mobile Robot	50
6.2.1 Down-Hill Gradeability	51
6.2.2 Cross-Hill Gradeability	51
Chapter 7 EQUATION OF MOTION	53
7.1 Second Order Lagrange Equation	53
7.2 Motion of Rover Suspension Mechanism	55
7.3 Equation of Motion of Linkage Mechanism with Three Degrees of Freedom	58
Chapter 8 COMPUTER SIMULATION	66
8.1 Rover Drive on Test Course	66
8.1.1 Hill Climbing	66
8.1.2 Step Climbing	68
8.2 Evaluation of Test Results	69

Chapter 9 CONCLUSION	70
REFERENCES	71
APPENDIX A – DIMENSIONS OF SUSPENSION MECHANISM AND ROVER	A1
APPENDIX B – CONSTRAINT FUNCTION SOLUTION	A2
APPENDIX C – POSITION ANALYSIS WITH MICROSOFT EXCEL	A4
APPENDIX D – KINEMATIC ANALYSIS WITH VISUAL NASTRAN	A5

LIST OF FIGURES

Figure 1-1	Sojourner examining the rock named “Yogi”	1
Figure 1-2	First Planetary Exploration Rover “Lunokhod”	4
Figure 1-3	NASA - JPL Sojourner Rover	5
Figure 1-4	Inflatable Rover	6
Figure 1-5	Rocky 7 Rover	6
Figure 1-6	Sample Return Rover - (SRR)	7
Figure 1-7	Nanorover with active suspension	7
Figure 1-8	Micro5 rover with suspension named Pegasus	8
Figure 1-9	Shrimp Rover designed by EPFL – Switzerland	9
Figure 1-10	Illustration of Mars Exploration Rover	9
Figure 1-11	Rocky terrain on the rim of crater Bonneville	10
Figure 2-1	Independent car suspension system with damper and spring	12
Figure 2-2	Definition of capacity	13
Figure 2-3	Free body diagrams of towed and driven wheels	13
Figure 2-4	Articulated Suspension System (US 4,840,394)	14
Figure 2-5	Kinematic diagram of Rocker-Bogie suspension	15
Figure 2-6	Wheel passing over same wheel diameter and more than half wheel diameter height obstacle	16
Figure 2-7	Bogie overturn problem	17
Figure 3-1	Watt’s linkage application on rear-suspension	18
Figure 3-2	Cross-link straight line mechanism by Chebyshev	19
Figure 3-3	Watt’s Approximate Straight-Line Mechanism	20
Figure 3-4	Robert’s Mechanism	20
Figure 3-5	Lambda Mechanism	21
Figure 4-1	Kinematic diagram and closed loops of bogie mechanism	25
Figure 4-2	Structural groups with different kinematic pairs	26
Figure 4-3	Structural synthesis with one input and one structural group	26
Figure 4-4	Structural synthesis of structural groups with zero degree of freedom ..	27
Figure 4-5	Closed kinematic chains with 4 and 5 structural groups	28
Figure 4-6	Structural synthesis of a four-bar mechanism	29
Figure 4-7	Structural synthesis of Lambda mechanism	29

Figure 4-8	Structural synthesis of double-lambda	30
Figure 4-9	Structural synthesis of bogie	30
Figure 4-10	Definition of linkages and crank angle	31
Figure 4-11	Trajectory of one wheel at different positions	32
Figure 4-12	First singularity of lambda mechanism where $\beta = 0^\circ$	33
Figure 4-13	Second singularity of lambda mechanism where $\beta = 180^\circ$	33
Figure 4-14	Connection between two lambda mechanisms, definition of ground clearance	34
Figure 4-15	Experimental suspension design LBS	35
Figure 4-16	Differential gear mechanism between right and left rockers	35
Figure 4-17	LBS kinematic diagram	36
Figure 4-18	Different applications of lambda bogie suspension	37
Figure 5-1	Description of position vector P	38
Figure 5-2	Vector loops on lambda mechanism	39
Figure 5-3	Angles between linkages	40
Figure 5-4	Graph of function P and geometrical trajectory	42
Figure 5-5	Transmission angle	43
Figure 5-6	Left side of the bogie mechanism	46
Figure 5-7	Singular configurations of right and left side of the bogie	48
Figure 6-1	Force diagram of LBS	49
Figure 6-2	Stability area consists of contact points	50
Figure 6-3	Downhill rear and front stability margins and dimensions	51
Figure 6-4	Lateral stability margins and dimensions	51
Figure 7-1	Equivalent forces and virtual displacements of LBS	56
Figure 7-2	Reverse step climbing first configuration	57
Figure 7-3	Reverse step climbing second configuration	57
Figure 7-4	Reverse step climbing third configuration	58
Figure 8-1	Rover computer model for simulation	66
Figure 8-2	Test course	67
Figure 8-3	Wheel reaction forces on test course	67
Figure 8-4	Course with small hill	68
Figure 8-5	Step climbing performance of LBS	68
Figure A.1.1	General dimensions of the rover (Front View)	A1

Figure A.1.2 General dimensions of the rover (Side View)	A1
Figure A.3.1 Screenshot of Microsoft Excel	A4
Figure A4.1 Visual Nastran screenshot	A5

Chapter 1

INTRODUCTION

On July 4, 1997, an orange coloured big ball softly bounced on the surface of Mars with an unusual robotic vehicle inside. This was the first planetary mission which has been wide public interest after first man on the moon. Small rover “Sojourner” conducted scientific experiments for 83 Sols (Mars Days) and took hundreds of photographs [1]. Roving on another planet came from dream to real by the help of science and patient ambitious research. This successful mission encouraged the scientists and NASA to continue the Mars exploration with new rovers.



Figure 1-1: Sojourner examining the rock named “Yogi” (Courtesy of NASA/JPL-Caltech)

Many rovers developed after Sojourner with different features and scientific objectives. In early days of January 2004, second and third rovers landed different locations on Mars named Spirit (MER1) and Opportunity (MER2) [2]. Scientific results of these powerful vehicles are bigger than their physical dimensions. All of the three rovers’ success and scientific results show that space agencies will continue robotic geologists frequently in future.

1.1 Mobile Robots and Description of “Rover”

1.1.1 Definition of Mobile Robot

Similar to the International Standards Organization’s definition of an industrial robot, mobile robot can be defined as;

“A mobile robot is an autonomous system capable of traversing a terrain with natural or artificial obstacles. Its chassis is equipped with wheels/tacks or legs and possibly a manipulator setup mounted on the chassis for handling of work pieces, tools or special devices. Various preplanned operations are executed based on a pre-programmed navigation strategy taking into account the current status of the environment.” [3]

This definition any intelligent machine which moves with respect to environment within limited human interaction (autonomously) called “Mobile robot”. Mobile robots can be classified by significant properties as;

- Locomotion (Legged, wheeled, limbless, etc.)
- Suspension (Rocker-bogie, independent, soft, etc.)
- Steering (Skid, Ackerman, explicit)
- Control Algorithm (Fully-Autonomous, semi-autonomous)
- Body Flexibility (Unibody, multibody)
- Usage Area (Rough Terrain, even surface, etc.)
- Guidance and Navigation (Star field or Sun detection, GPS, sensor-based)

Mobile robots can be used in several applications. Dangerous area operations (Nuclear plants), planetary exploration and pipe investigation, extreme temperature and narrow field investigations (pyramid exploration robots). Moreover, floor cleaning robots and servant robots are common examples for indoor use. It is not a dream that, in near future robots will be a part of our daily life.

1.1.2 Locomotion

Locomotion is a process, which moves a rigid body. There is no doubt that a mobile robot's most important part is its locomotion system which determines the stability and capacity while traversing on rough terrain. The difference of robotic locomotion is distinct from traditional types in that it has to be more reliable without human interaction. While constructing a robot, designer must have decided on the terrain requirements like stability criteria, obstacle height, and surface friction. There is no only one exact solution while comparing the mobility systems. [3, 4]

There are several types of locomotion mechanisms were designed depending on nature of the terrain. Locomotion systems can be divided into groups as; wheeled, tracked, legged (walking robots), limbless (snake and serpentine robots) and hopping robots. Wheeled rough terrain mobile robots are called as "Rover".

In nature, insects are the fastest creatures, comparing to body/speed with their numerous legs. There is no suspicion that we are going to see legged robots more frequently in future with improved leg control algorithms and new lightweight materials. Limbless locomotion is another terrain adaptive locomotion type for reptile creatures. Snakes can move very fast on uneven terrain, additionally, they can easily climb on trees by their highly flexible body structure.

Although animals and insects do not use wheels, wheeled locomotion has several advantages for human-made machines. Rovers can carry more weight with high-speed comparing to walking robots and snake robots. Another advantage of wheeled locomotion is navigation. Wheeled robot's position and orientation can be calculated more precisely than tracked vehicles. Opposite to wheeled locomotion, legged locomotion needs complex control algorithms for positioning.

1.2 History of Rovers

1.2.1 Lunakhod

The first planetary exploration rover was “Lunakhod” which has been sent Moon 2 times with USSR – Luna missions to gather information around landing site and send pictures of terrain.

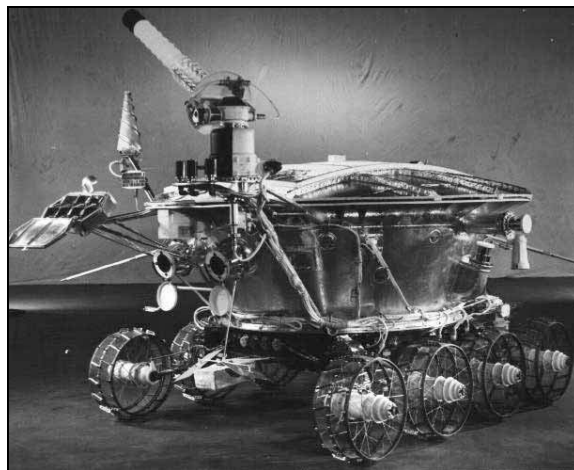


Figure 1-2: First Planetary Exploration Rover “Lunokhod” (Courtesy of Lavochkin Assoc.)

Lunakhod has guided in real-time by a five-person team at the Deep Space Center near Moscow, USSR. Lunakhod-2 toured the lunar Mare Imbrium (Sea of Rains) for 11 months in one of the greatest successes travelled 37 km on Moon surface.

1.2.2 Sojourner

In 1996, NASA – Jet Propulsion Laboratory and California Institute of Technology have designed new rovers with identical structure named Sojourner and Marie-Curie. These small rovers were only 10.5 kilograms and microwave oven sized. Rover Sojourner launched with Pathfinder landing module in December 1996. Marie Curie rover was also planning to send Mars with 2001 mission which has been cancelled [11, 15].

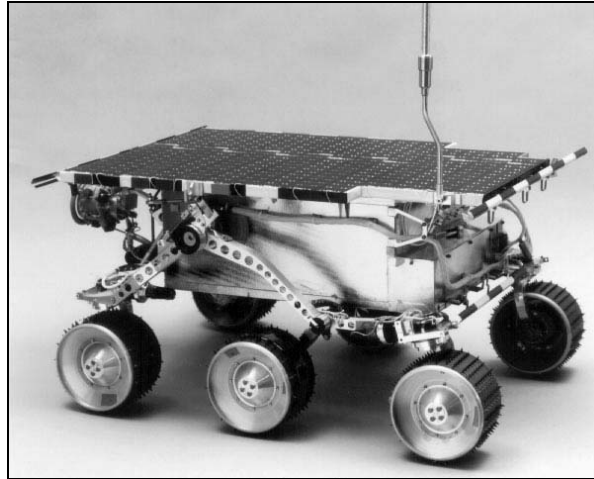


Figure 1-3: NASA - JPL Sojourner Rover (Courtesy of NASA/JPL-Caltech)

Operators have sent commands via lander Pathfinder and they examined rocks and soil components of Mars more than 3 months. Sojourner was a breaking point of exploration rovers with its unique six-wheeled suspension system which can overcome one and a half wheel diameter height obstacles that is similar to an automobile passing over a table sized obstacle.

1.2.3 Inflatable Rover

Another alternative to move on a harsh environment is to have big wheels. If a rover has large wheels compared to obstacles, it can easily operate over most of the Martian rocky surface. Researches show that inflatable rover with 1.5 meter wheel diameter can traverse 99% of the area [16]. Inflatable rover has 3 wheels which are driven by motors.



Figure 1-4: Inflatable Rover (Courtesy of NASA/JPL-Caltech)

Robot could be able to travel approximately 30 km per hour on Mars surface by its 100-watt power.

1.2.4 Rocky 7

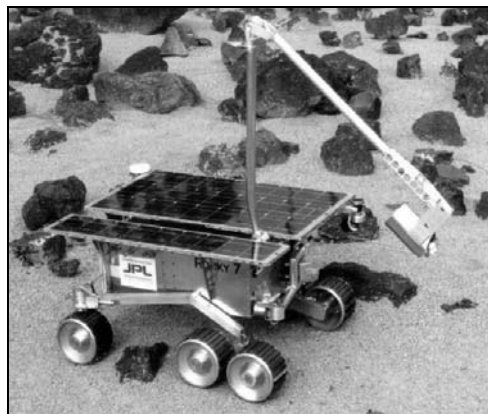


Figure 1-5: Rocky 7 Rover (Courtesy of NASA/JPL-Caltech)

Rocky 7's design and dimensions are similar to Sojourner. A robotic arm is attached to the body for investigation. Mobility system changed to 2-wheel steering similar to Ackerman type [27]. Although this modification decreases the complexity for control systems, maneuverability is restricted.

1.2.5 Sample Return Rover

Rough terrain mobility of a mobile robot can be increased by center of gravity shifting methods. A good example to this category is NASA Sample Return Rover (SRR) which has been designed to collect soil and stone sample from Mars surface. SRR has active suspension system with variable angle between linkages [28].



Figure 1-6: Sample Return Rover - (SRR) (Courtesy of NASA/JPL-Caltech)

On inclined surface, active suspension can hold the main body horizontal. Navigation gets easier by this feature of rover.

1.2.6 Nanorover

Another example to active suspension system is nanorover which was designed for exploration of small celestial bodies like comets and asteroids. Small dimensions and lightweight are advantages of this robot.

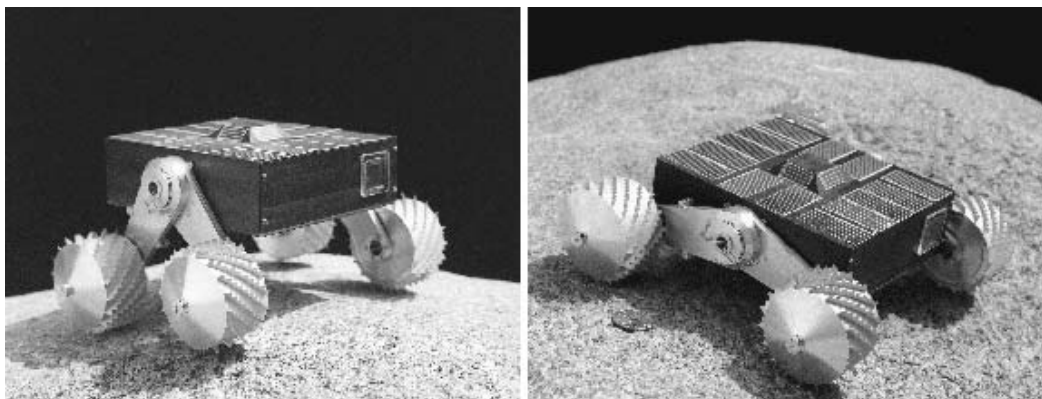


Figure 1-7: Nanorover with active suspension (Courtesy of NASA/JPL-Caltech)

Mobility system consists of four wheels with 6 cm diameter. Each wheel connected to the chassis with independent positioned struts. Since the robot can operate on both sides (upside-down), overturning is not a problem. Onboard computer can manipulate the suspension to arrange traction forces [29].

1.2.7 Micro5

Japanese Lunar rover Micro5 is a five-wheeled rover. Suspension system named Pegasus; uses a fifth wheel to support the remaining wheels while front wheels climbing obstacles. The rover with 100 mm wheel diameter is able to climb 150 mm height steps and rocks [34].



Figure 1-8: Micro5 rover with suspension named Pegasus
(Courtesy of Meiji University – Japan)

Pegasus mobility system has 4 active wheels and one extra wheel which is connected to the body with an actuated joint. When front wheels climb, the fifth wheel carries some part of the weight to help wheels.

1.2.8 Shrimp

Shrimp is another six-wheeled rover which designed by Swiss Federal Institute of Technology – EPFL. It has a one front four-bar to climb over obstacles up to two-wheel diameter without any stability problem. Middle four wheels have parallelogram

bogie which balances the wheel reaction forces during climbing. Single rear wheel connected directly to the main body also driven by motor to increase the climbing capacity. [14]

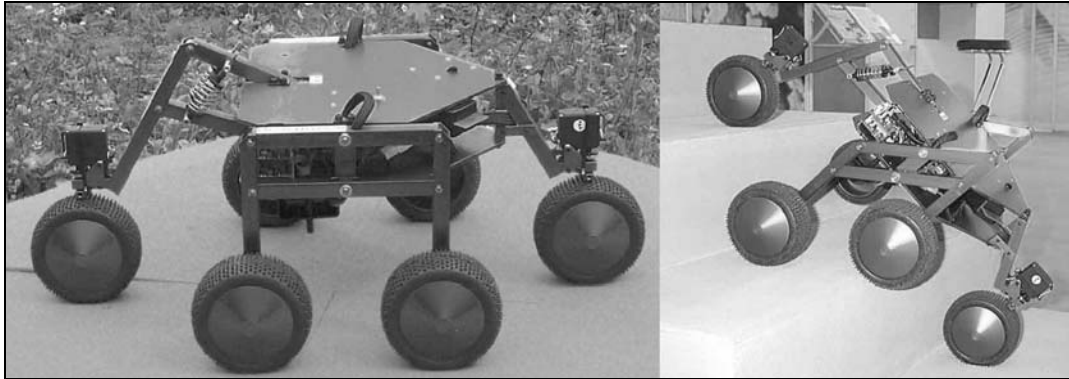


Figure 1-9: Shrimp rover designed by EPFL – Switzerland (Courtesy of EPFL)

1.2.9 Mars Exploration Rovers (MER)

Mars Exploration Rovers are developed designs of Sojourner. Each Mars Exploration Rover is 1.6 meter long and weighs 174 kilograms. Opposite to previous rover Sojourner, which was commanded via lander Pathfinder, these robots carry all required electronic devices on their body. Mobility system is similar to Sojourner rover with Rocker-Bogie suspension and 4-wheel steering. [2]



Figure 1-10: Illustration of Mars Exploration Rover (Courtesy of NASA/JPL-Caltech)

1.3 Rover Operations and Future Requirements

Today's rovers are driven by commands which are sent from ground operators after tested in 3D computer simulator. Some of the critical motions such as climbing high slope, driving near crater rim between rocks which have variety of height, rover motions must be taken under consideration of flight engineers. These operations are need to be decided by a large operator group, which increases the total cost of the planetary exploration project.



Figure 1-11: Rocky terrain on the rim of crater Bonneville (Courtesy of NASA/JPL-Caltech)

As the future space exploration trend includes less cost principle, new rover designs are needed to be more flexible during field operations. Although obstacle detection and avoidance algorithms decrease the average speed, restriction of the overall speed is suspension design of the vehicle. For example, the Mars Exploration Rovers have a top speed on flat hard ground of 5 centimetres per second. To increase the safety of the drive, the rover has hazard avoidance software which causes to stop and re-evaluate its position every few seconds. Because of the safety procedures in the field operations, the average speed can go up to 1 centimeter per second [10]. It is non-avoidable fact that future rovers will reach high speed compared to current speed with software improvements and with the suspension design.

Chapter 2

WHEELED LOCOMOTION AND SUSPENSION

Like all other design matters in engineering, robots are designed according to its working environment and purpose. Generally, wheeled robots have advantages on rough, sandy surface with carrying large bodies. Moreover, wheeled robots can rotate even on a spot without any skidding.

2.1 Suspension

Wheeled locomotion's main component is its suspension mechanism which connects the wheels to the main body or platform. This connection can be in several ways like springs, elastic rods or rigid mechanisms. Most of the heavy vehicles like trucks and train wagons use leaf springs. For comfortable driving, cars use a complex spring, damping and mechanism combination. Generally, exploration robots are driven on the rough surface which consists of different sized stones and soft sand. For this reason, car suspensions are not applicable for rovers. The requirements of a rover suspension are;

- As simple and lightweight as possible
- Connections should be without spring to maintain equal traction force on wheels
- Distribute load equally to each wheel for most of the orientation possibilities to prevent from slipping

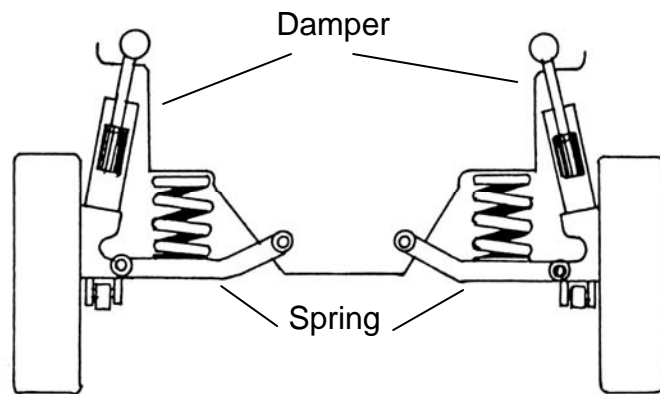


Figure 2-1: Independent car suspension system with damper and spring

Soft suspension systems with spring reduce vibrations and effects of impacts between wheel and ground. However, reaction force of pressed spring increases the force that transmits from wheel to ground. When climbing over an obstacle, higher wheel's traction force is more than the lower one which causes slippage.

2.2 Obstacle Capacity

A rover's obstacle limit generally compared with robot's wheel size. In four wheel drive off-road vehicles, limit is nearly half of their wheel diameter [4]. It is possible to pass over more than this height by pushing driving wheel to obstacle which can be called as *climbing*. Step or stair climbing is the maximum limit of obstacles. The contact point of wheel and obstacle is at the same height with wheel center for this condition.

Field tests show that Mars mobile robots should be able to overcome at least 1.5 times height of its wheel diameter. This limitation narrows the mobile robot selection alternatives and forces scientists to improve their current designs and study on new rovers.

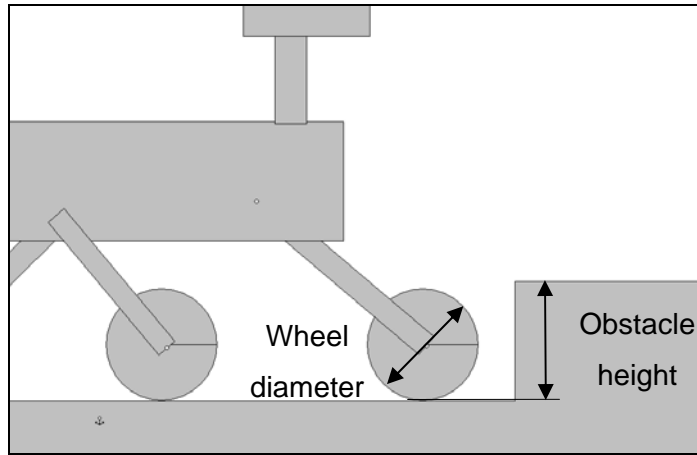


Figure 2-2: Definition of capacity

Former rover designs have different capacities. The rocker-bogie suspension which has been used on NASA Sojourner, Spirit and Opportunity rover can pass over 1.5 wheel diameter obstacles. The “Shrimp III” rover has extensive ability with a climbing wheel connected by rhombic four-bar has 2 wheel diameter height step obstacle capacity [14]. Although powerful climbing characteristics, rover’s stability loses its advantage while driving down slope.

All these researches show that most of the rover designs have a climbing capacity between 1.5 diameters and 2 diameters of wheel. To reach higher capacities, active climbing methods are required.

2.3 Wheel Forces

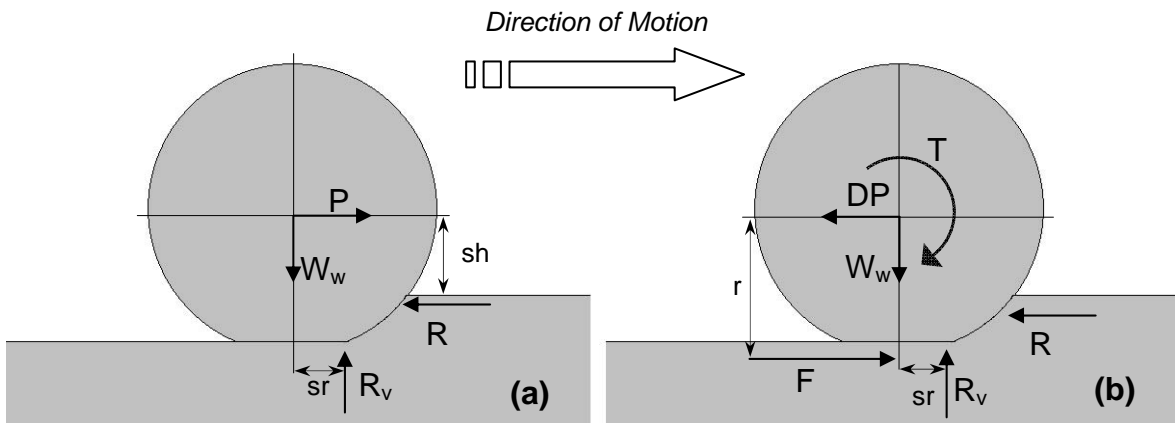


Figure 2-3: Free body diagrams of towed (a) and driven (b) wheels [26]

A rigid wheel sinks on the soft terrain as in figure 2-3. sh distance is called sinkage height. Geometry of wheel, material and ground stiffness affect sinkage height. Depending on the geophysical properties of soil, different reaction and resistance forces act on wheel.

The towed wheel carries some part of body weight (W_w). The force P which tries to move the wheel, acts from vehicle axis to center point of the wheel. These two forces are balanced by vertical ground reaction force (R_v) and resistance force of soil R . In towed wheel, resistance force has to be as small as possible. Motion resistance force is resultant of soil compaction resistance, bulldozing resistance, rolling resistance, gravitational resistance and obstacle resistance.

On the driven wheel, additional traction force F acts to the contact point with the same direction of motion. Traction force tries to pull the chassis of robot.

2.4 Rocker-Bogie Suspension

Rocker-Bogie suspension has been developed for first Mars rover Sojourner by NASA – JPL [19].

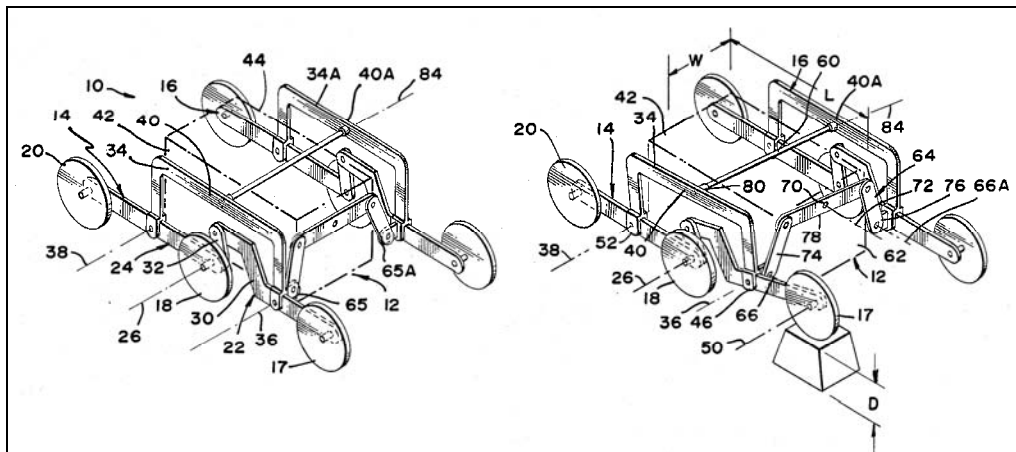


Figure 2-4: Articulated Suspension System (US 4,840,394)

This suspension has 6 wheels with symmetric structure for both sides. Each side has 3 wheels which are connected to each other with two links. Main linkage called *rocker* has two joints. While first joint connected to front wheel, other joint assembled to another linkage called *bogie*, which is similar to train wagon suspension member. In later design of articulated suspension system, called rocker-bogie with small changes.

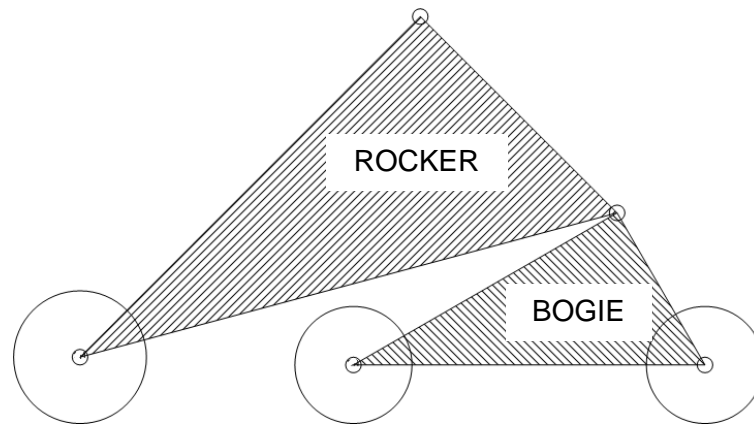


Figure 2-5: Kinematic diagram of Rocker-Bogie suspension

The main advantage of the rocker bogie suspension is load on each wheel is nearly identical. On different positions, wheels' normal force equally distributes contrary to 4 wheel drive soft suspensions [4].

The connection between symmetrical lateral mechanisms is provided by a differential mechanism which is located inside the body. Rotation of axles which are connected two rockers are averaged, thus, vehicle body pitch angle always adapted even if one side steps over obstacle.

2.5 Wheel Motion

While driving on a flat surface, if there is no slipping, wheel center will move on a line parallel to the surface with constant velocity. Although, obstacle geometries can be different, most difficult geometry which be can climbed by wheel is stair type rectangular obstacle.

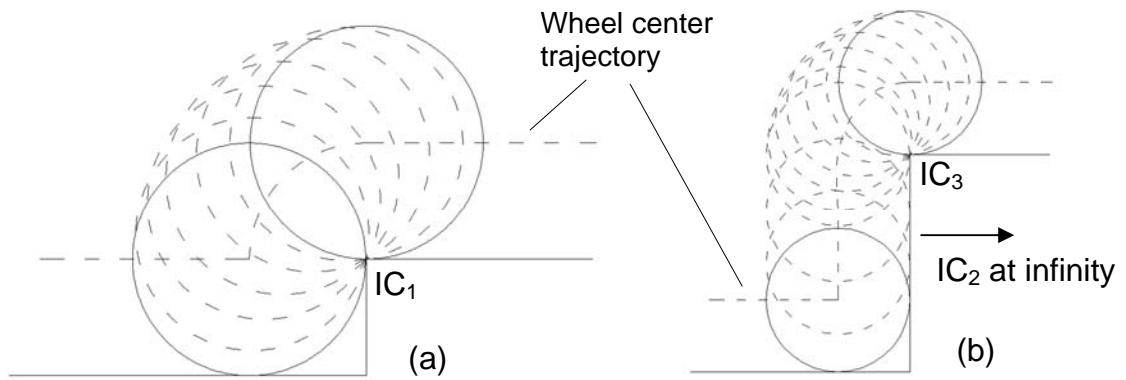


Figure 2-6: Wheel passing over same wheel diameter (a) and more than half wheel diameter (b) height obstacle

In figure 2-6(a), height of the obstacle is same or less than the half diameter of the wheel. For this condition, the wheel's instant center of rotation (IC_1) is located at the contact point of the obstacle and wheel. Trajectory of the wheel centers' during motion generates a soft curve, thus, horizontal motion of the wheel center does not break.

Since in figure 2-6 (b), height of the obstacle is more than the half diameter of wheel, this condition can be classified as *climbing*. Climbing motion consist of two sub motions. First one is a vertical motion, which causes a horizontal reaction force on wheel center . This vertical motion's instant center (IC_2) is at infinity. Second one is a soft rotation similar to figure 2-6 (a) with instant center of rotation (IC_3) at the corner.

2.6 Advantage of Linear Motion

Although, load distribution advantage of rocker-bogie, a critical problem can occur when climbing over an obstacle. Wheel forces on opposite direction of motion produce a moment about pivot joint to rotate bogie.

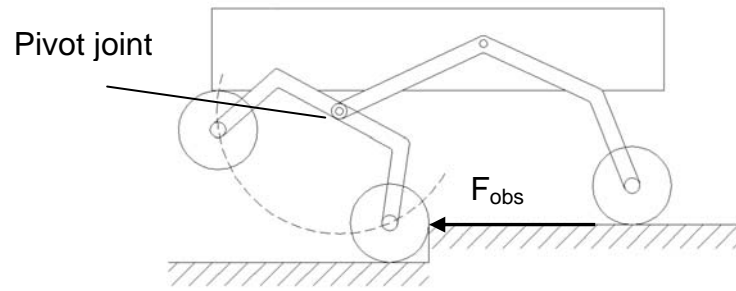


Figure 2-7: Bogie overturn problem

As we discuss in wheel forces, there are several forces act on wheel on x axis. If the surface friction of an obstacle is not enough to climb, obstacle force (F_{obs}) can reach high values. This problem can also occur while middle wheel actuator failure. Driving velocity is also restricted by bogie overturn problem. Bogie pitch angle can be adjusted by active control methods [35].

An easy solution method for this problem can be a linear motion suspension usage where obstacle reaction force cannot create any moment.

Chapter 3

STRAIGHT LINE MECHANISMS

In machine science, it is important to generate special curves, exact circular motion and straight line. Dimensional synthesis theories are used to generate a special curve with coupler. There are different analytical and graphical synthesis methods for motion generation, function generation and path generation.

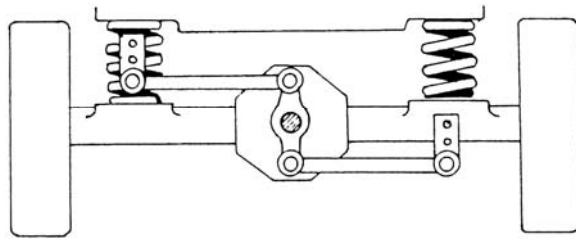


Figure 3-1: Watt's linkage application on rear-suspension

Linear motion mechanisms have wide usage area in suspension mechanism design. Most of the suspension members are needed to move on a straight line for lateral motion of an axle [5]. In theoretically, a four-bar mechanism generates a coupler curve in 6th order equation. Some portion of this curve can be close to a theoretical line with small deviation which can be neglected [6]. Usually, these mechanisms generate linear motion from a rotational motion of a crank. For this kind of design, force transmits from crank to coupler. In suspension designs, force is applied from ground to coupler. This force generates a moment on crank that balanced with a spring's reaction force.

3.1 Chebyshev Mechanism

Chebyshev mechanism consists of double symmetric rockers connected with a coupler with a coupler point E is midpoint of coupler link. Trajectory of point E is

approximately linear. Limited useful range is the most important disadvantage of this mechanism.

Favorable parameters are;

$$c = 1, a = 0.5, b = d = 1.25$$

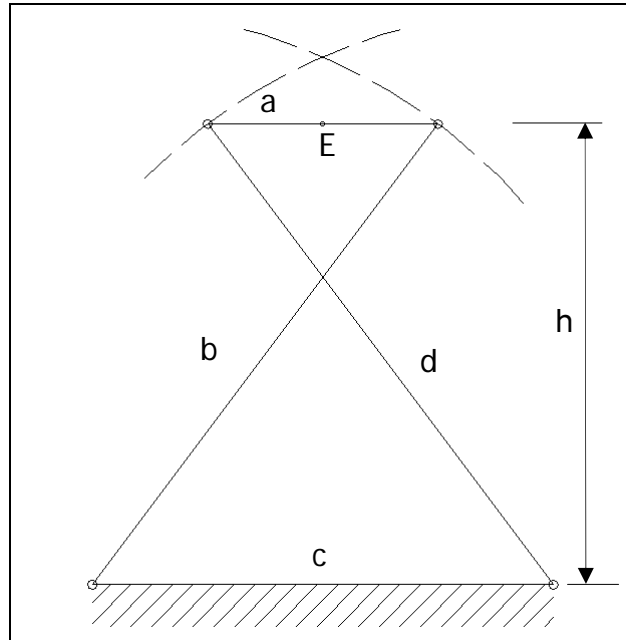


Figure 3-2: Cross-link straight line mechanism by Chebyshev

The straight line is parallel to the fixed base. The distance between these lines is

$$h = 1$$

3.2 Watt's Linkage

Watt's linkage is also another four-bar mechanism which generates an *approximate straight line* on a plane. It is also called "*Lemniscoid*" because of the trace of the coupler point similar to "8" curve.

Recommended dimensions are [7, 13];

$$a = c = 30 \text{ and } b = 50$$

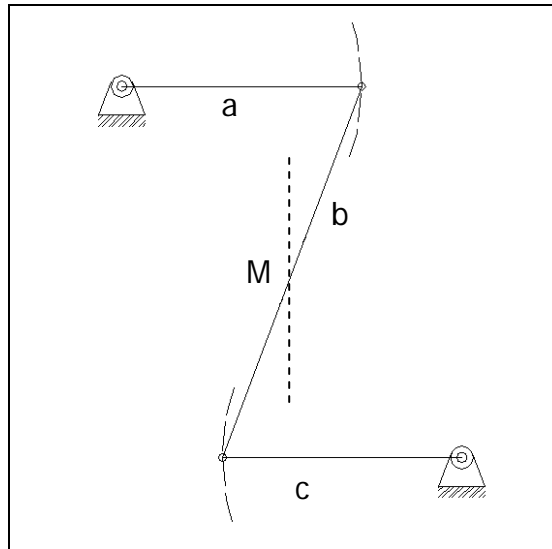


Figure 3-3: Watt's Approximate Straight-Line Mechanism

3.3 Robert's Linkage

Robert's linkage is another four-bar approximate straight line generator mechanism with coupler point C. Good results can be obtained with construction parameters $d = 1$, $b = 0.538$, $a = c = 0.530$ $e = f = 1.04$

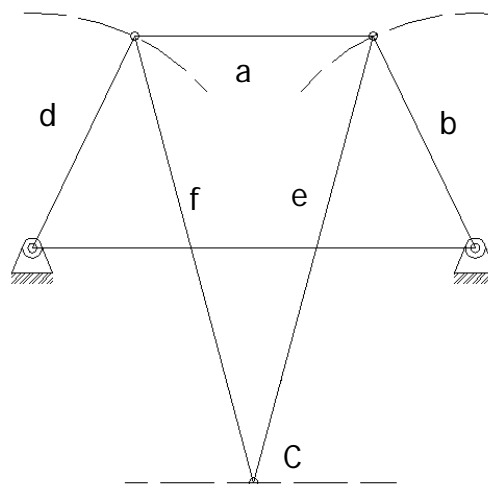


Figure 3-4: Robert's Mechanism

Robert's mechanism generates a curve which has a linear part parallel to the base link. Links and coupler curve are symmetric.

3.4 Chebyshev's Lambda Mechanism (Hoeken Mechanism)

Although, most of the books named Hoeken mechanism [7, 49, 50]; the first definitions of lambda (λ) mechanism are proposed by famous mathematician Chebyshev, Pafnuty Lvovich in 1869 [8, 9, 12].

Lambda mechanism is another four-bar straight line generator. Crank link can rotate 360 degrees while the coupler point moves on coupler curve. Curve has two characteristic motions. First part is straight line and second part is a quick return curve.

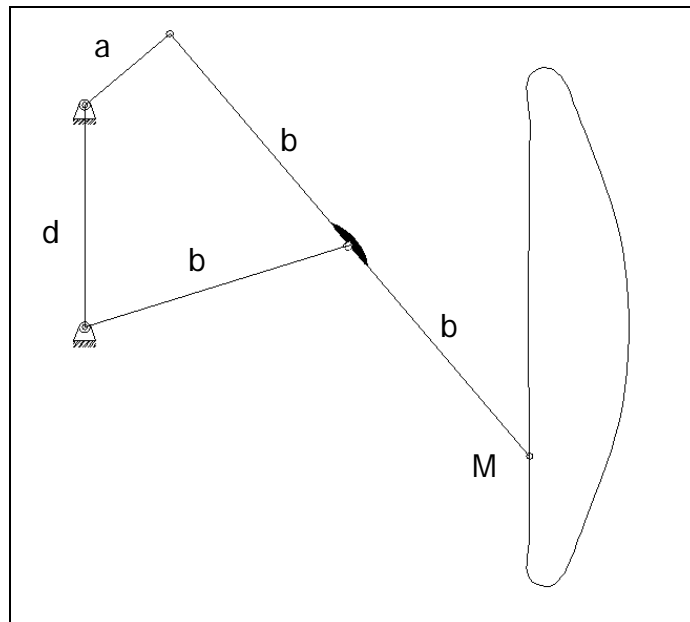


Figure 3-5: Lambda Mechanism

Chebyshev's mechanism is defined by three independent parameters;

a, b and d

To move the coupler point M, along a line sufficiently and necessary to fulfil the relation:

$$3d - a = 2b$$

In this relation, symmetrical coupler curve of point M has six points of intersections with the ideal line. The extreme deviation is reached seven times with subsequently changing signs.

The length of fixed d can be changed according to relation;

$$1.55a \leq d \leq 3a$$

If $d = 3a$ and $b = 4a$, triangle BDC equilateral triangle in the middle position of the mechanism.

If $d = 2.22$, ratio of maximum error from straight line to the length of straight line will not be more than 0.001 that is if $L = 100$ mm, the error will not be more than 1 mm. [8, 12]

Chapter 4

STRUCTURAL SYNTHESIS AND DESIGN OF SUSPENSION MECHANISM

Design of a robotic system starts with *structural synthesis* where researcher can find the answer of mobility and capability of intended mechanism. Structural and mobility analysis formulas are important and popular subjects of kinematics.

4.1 Structural Synthesis

4.1.1 Mobility Analysis

Mobility or *degree of freedom* (DOF) of a mechanism is the number of *independent* parameters or inputs needed to specify the configuration of a mechanism completely. There are many mobility formulas have been developed to explain degree of freedom of a mechanism in terms of number of links, number of joints and joint types [17].

Most famous one of these formula is Grübler (1885) [20, 21] criteria;

$$W = \lambda(n - j - 1) + \sum_i f_i \quad (4.1)$$

where;

W: degrees of freedom of mechanism

λ : degrees of freedom of the space in which mechanism intended to function

n: number of links in a mechanism (including the fixed link)

j: number of joints

f_i : degrees of relative motion permitted by joint i

Another interesting formula has been presented for structural formula DOF with *variable general constraint* by F. Freudenstein and R. Alizade in 1975 [22];

$$W = \sum_{i=1}^j f_i - \sum_{k=1}^L \lambda_k \quad (4.2)$$

$\lambda = 6$ for space

$\lambda = 3$ for plane and spherical workspace

$\lambda = 2$ for plane with one constraint (Cartesian motion without rotation)

In 1988, R. Alizade has introduced a new structural formula with *constant general constraint* for the platform type mechanisms and manipulators for mobility of all kinematic pairs [23];

$$W = \sum_{i=1}^j f_i - \lambda(N - C - B) \quad (4.3)$$

where;

W: Degrees of freedom of mechanism

N: Total number of joints on the platforms

B: Number of platforms

C: Total number of intermediate branches between platforms

If there is *no platform* on the mechanism ($B = 0$), we can re-write equation (4.3);

$$W = \sum_{i=1}^j f_i - \lambda(N - C) \quad (4.4)$$

parameters become;

N: Number of joints on base link

C: Constraints between base links

4.1.2 Structural Synthesis Formula for Lower and Higher Kinematic Pairs

Let we introduce a new formula for *structural synthesis* of mechanism with lower and higher kinematic pair by using equation (4.2);

$$W = \sum f_l + 2 \sum f_h - \lambda(N - C - B) \quad (4.5)$$

where;

N: Number of joints on the base link or platform

f_h : Number of higher kinematic pairs

f_l : Number of lower kinematic pairs

If we construct new bogie by adding two lambda mechanism symmetrically, kinematic diagram will be as *figure 4-1*.

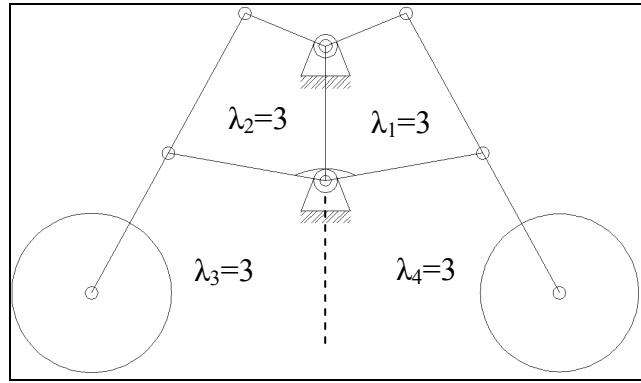


Figure 4-1: Kinematic diagram and closed loops of bogie mechanism

When we apply this formula on our new bogie;

$$\lambda = 3, f_l = 9, f_h = 2, L = 4$$

We can write the following equation from (4.5) for planar mechanisms as;

$$W = \sum f_l + 2 \sum f_h - \sum_{k=1}^L \lambda_k \quad (4.6)$$

where

L: Number of loops

For spatial mechanisms ($\lambda = 6$) equation (4.6) becomes;

$$W = \sum f_l + 5 \sum f_h - \sum_{k=1}^L \lambda_k \quad (4.7)$$

If we calculate degree of freedom of bogie;

$$W = 9 + 2 \cdot 2 - (3 + 3 + 3 + 3) = 1$$

Physically this equation proves that, one actuator is enough to move bogie on the ground.

4.1.3 Structural Groups

Structural group is a kinematic chain with zero degree of freedom (DOF) which cannot be divided into smaller structural groups with zero DOF ($W=0$).

Let $K = 1$, $W = 0$, $\lambda = 3$ we have,

$$f_l + 2f_h - 3 = 0 \quad \text{or} \quad f_l + 2f_h = 3$$

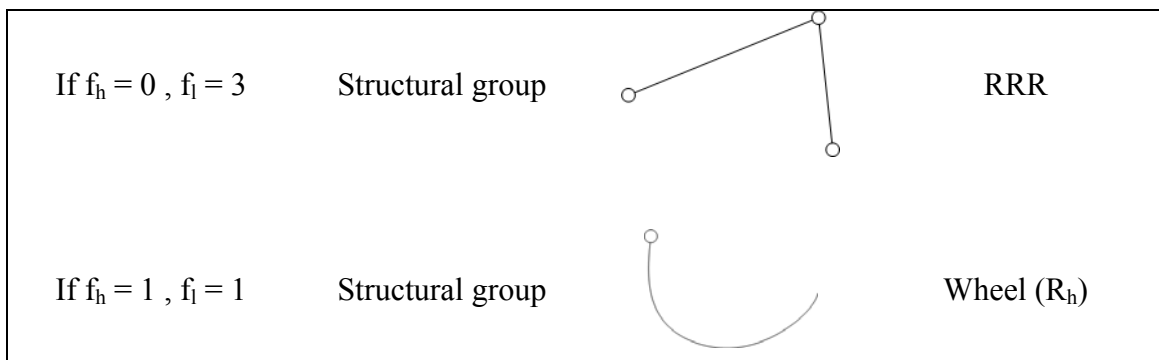


Figure 4-2: Structural groups with different kinematic pairs

Mechanism can be described by an input and a structural group.

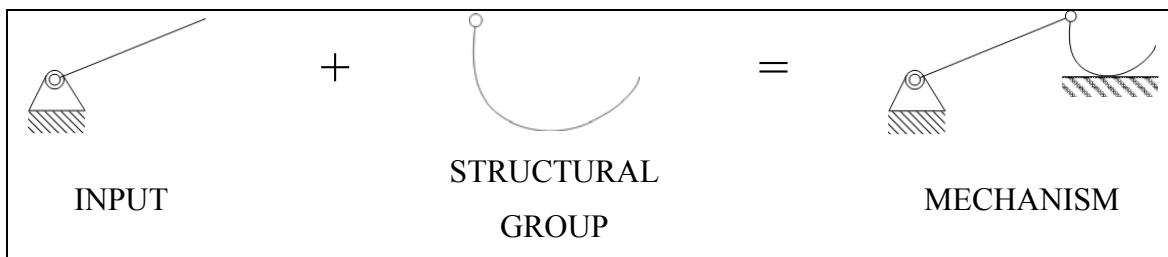


Figure 4-3: Structural synthesis with one input and one structural group

High kinematic structural group can be connected with input by elements of higher kinematic pairs. Structural groups cannot be divided into other structural groups with $W = 0$

Let $K = 2$, $W = 0$, $\lambda = 3$

$$f_l + 2f_h = 3 + 3 = 6$$

$$f_l + 2f_h = 6$$

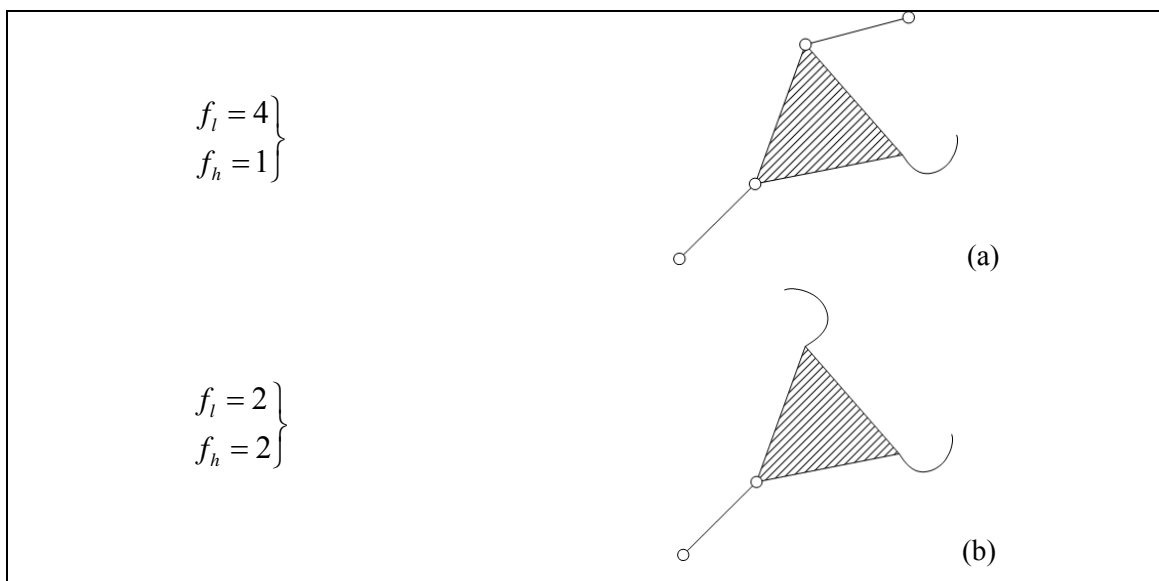


Figure 4-4: Structural synthesis of structural groups with zero degree of freedom

4.1.4 Closed Chain Construction with Structural Groups

If structural groups added each other as a chain, this mechanism always has zero mobility. We can calculate mobility of structural group which consist of $f_h = 1$, $f_l = 1$ by using (4.6);

$$W = \sum f_l + 2 \sum f_h - \sum_{k=1}^L \lambda_k = 1 + 2 - 3 = 0$$

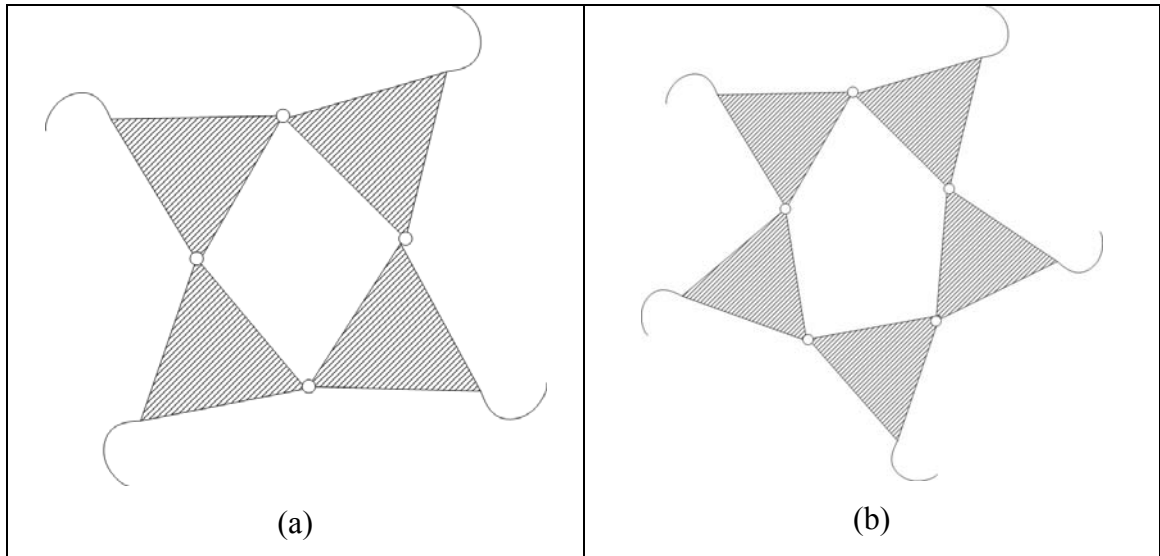


Figure 4-5: Closed kinematic chains with 4 (a) and 5 (b) structural groups

In figure 4-5 we constructed closed chains of structural groups. By applying (4.6) to both of the chains;

For figure 4-5(a);

Number of lower pairs $f_l = 4$

Number of higher pairs $f_h = 4$

Number of independent loops $L = 4$

Parameter of workspace $\lambda = 3$

$$W = \sum f_l + 2 \sum f_h - \sum_{k=1}^L \lambda_k = 4 + 2 \cdot 4 - 4 \cdot 3 = 0$$

For figure 4-5(b);

Number of lower pairs $f_l = 5$

Number of higher pairs $f_h = 5$

Number of independent loops $L = 5$

Parameter of workspace $\lambda = 3$

$$W = \sum f_l + 2 \sum f_h - \sum_{k=1}^L \lambda_k = 5 + 2 \cdot 5 - 5 \cdot 3 = 0$$

4.1.5 Structural Synthesis of Bogie Mechanism

Let us construct lambda mechanism by adding kinematic elements;

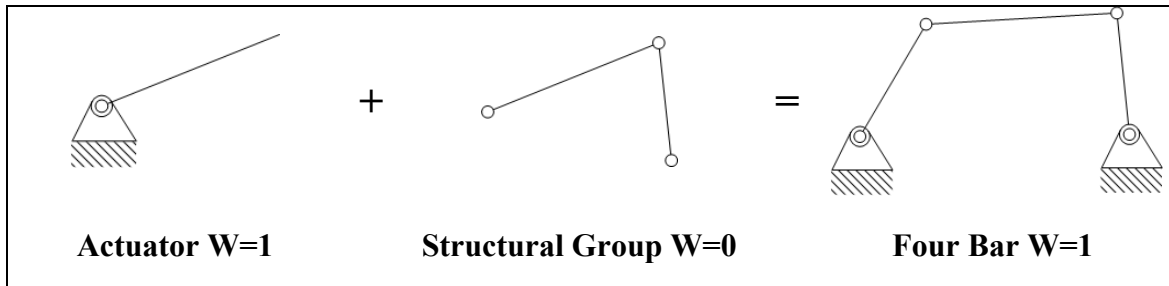


Figure 4-6: Structural synthesis of a four-bar mechanism

Adding a higher pair to a four-bar mechanism gives a lambda mechanism. For our design, higher pair is a wheel with a point contact with ground.

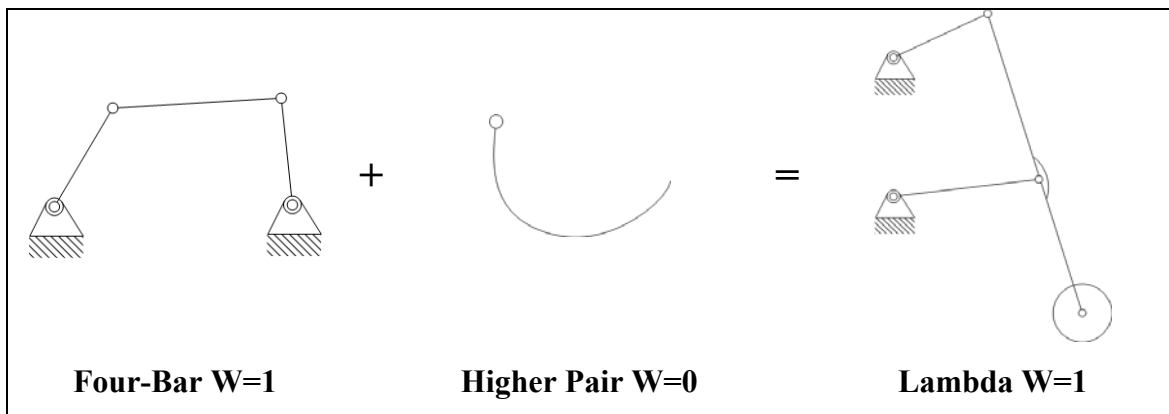


Figure 4-7: Structural synthesis of Lambda mechanism

This synthesis shows that Chebyshev's lambda mechanism has 1 DOF on plane. Let us add another structural group which has zero DOF to lambda mechanism.

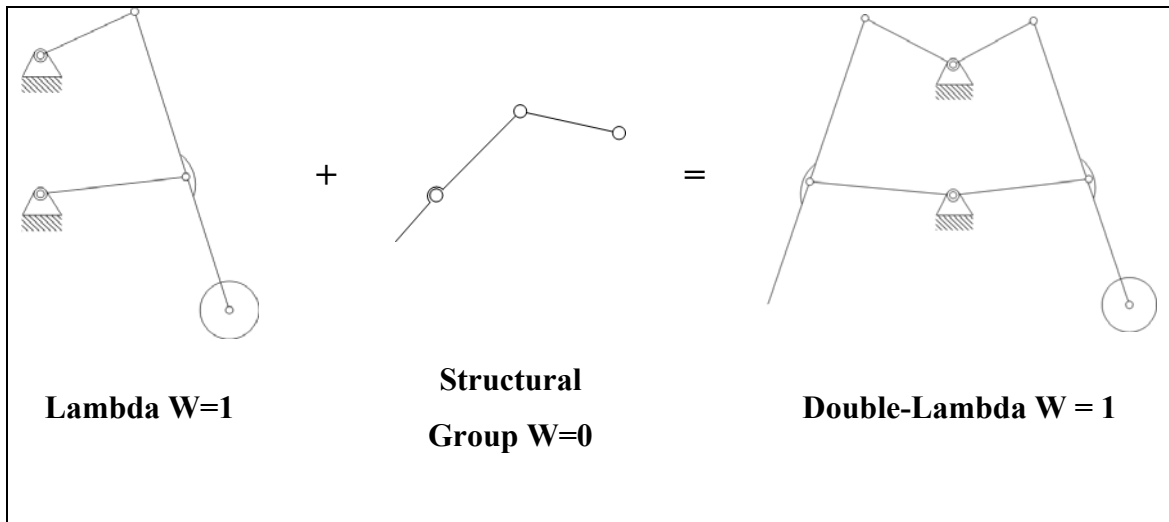


Figure 4-8: Structural synthesis of double-lambda

If we add another higher pair to double-lambda mechanism, we get bogie mechanism shown in figure 4-9.

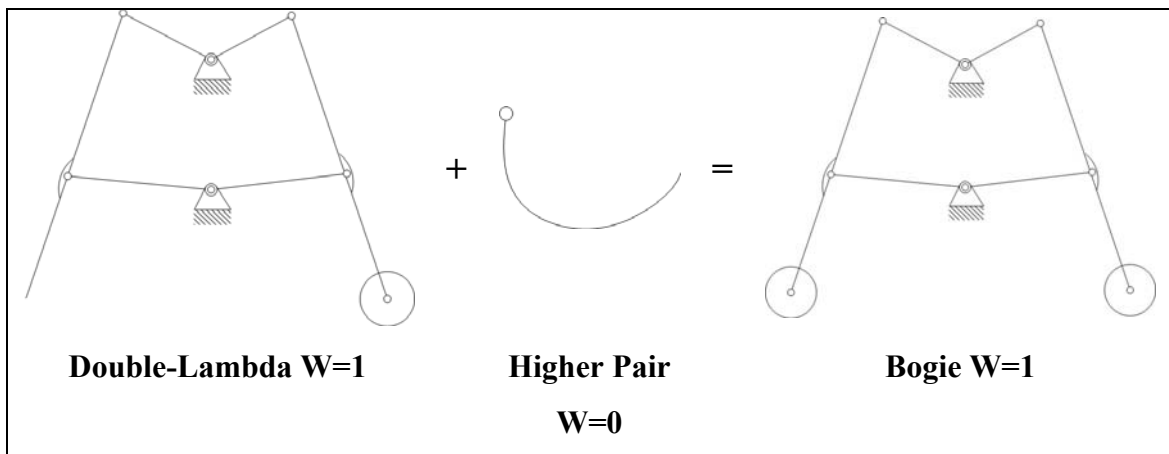


Figure 4-9: Structural synthesis of bogie

4.2 Design

4.2.1 Design Parameters Selection

Design parameters can be selected from Chebyshev's definitions which have been described in previous chapter. Our purpose is to maximize the linear part of the curve. This result can be achieved by selecting the parameters as;

$$1.55a = d$$

If we put $d = 1.55a$ into equation that yields;

$$3d - a = 2b$$

$$3 \cdot 1.55a - a = 2b$$

$$b = 1.825a$$

Comparing to overall size of rover we can assume $b = 200$ mm to design a mechanism.

That gives us;

$$a = 109 \text{ mm}$$

$$b = 200 \text{ mm}$$

$$d = 169 \text{ mm}$$

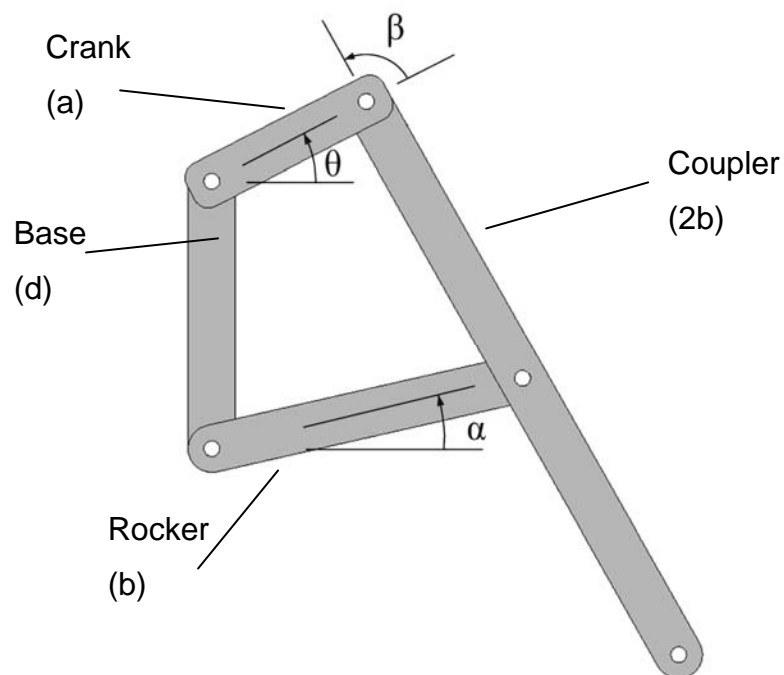


Figure 4-10: Definition of linkages and crank angle

4.2.2 Geometric Trajectory of Lambda Mechanism

By using these parameters, the instant positions and trajectory of lambda mechanism can be drawn as below

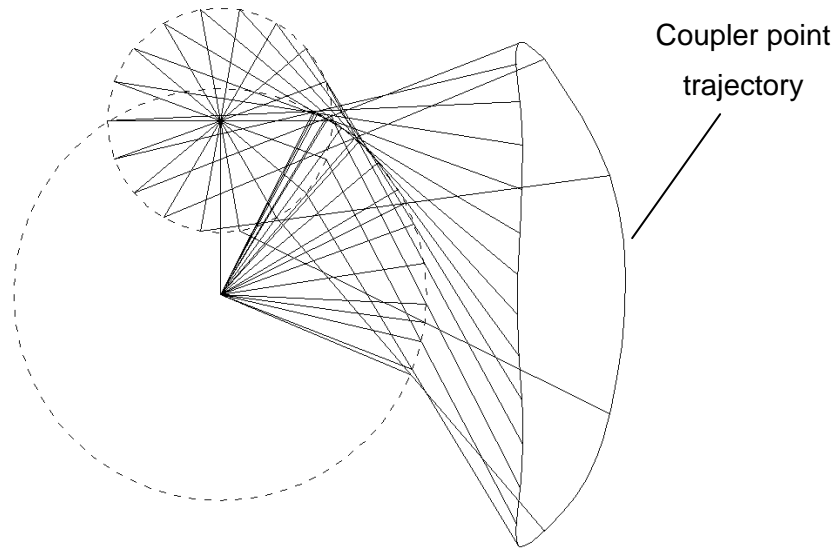


Figure 4-11: Trajectory of one wheel at different positions

Mechanism works linear in approximately 260 degrees angular displacement of crank. During this motion link B displacement is 80 degrees. This linear part with 490 mm vertical distance is the workspace of the double lambda mechanism. *Return motion* of the coupler curve will be out of our study.

4.2.3 Singularity

If a mechanism gets into position where displacement of output link is undefined or impossible with driving force of input link, this condition called *dead position* or *singularity* [18]. Four-bar mechanism gets singularity if transmission angle β reaches 0 or 180 degrees where input link (coupler) cannot transmit force to output link (rocker). This problem can be solved with help of other link or inertia effects. If another force applied from rocker to coupler, mechanism can continue its motion. For our bogie design we have to avoid from singular positions near workspace in order to transmit force from one lambda mechanism to other. If one side gets singular angle, whole mechanism will lock.

Lambda mechanism has two singular configurations like other four-bar mechanisms.

4.2.3.1 First Singularity

First singularity of lambda mechanism is reached when transmission angle (the angle between crank and coupler) $\beta = 0$ degrees. Although this angular position within the linear part of the coupler curve, this configuration is the upper limit of our suitable workspace.

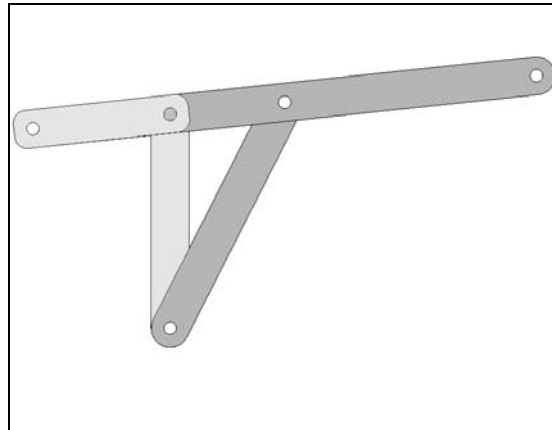


Figure 4-12: First singularity of lambda mechanism where $\beta = 0^\circ$

4.2.3.2 Second Singularity

Second singular position of lambda mechanism is reached when transmission angle $\beta = 180$. This configuration is on the end of linear part of the curve for this reason the lower limit of crank is that configuration.

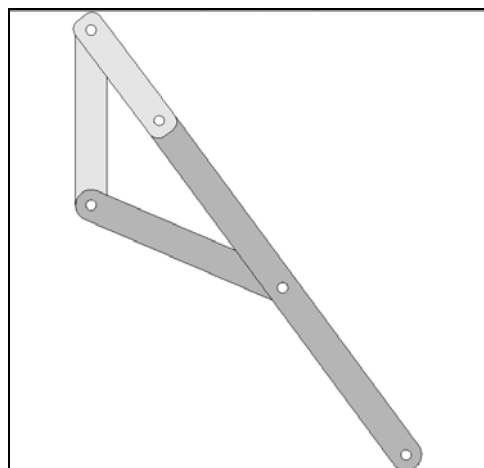


Figure 4-13: Second singularity of lambda mechanism where $\beta = 180^\circ$

4.2.4 Double-Lambda Mechanism Connection

New bogie design consists of two lambda mechanisms which are connected symmetrically. Thus, wheels move on a *straight line* but in *opposite direction* of each other. This design balances the reaction forces on each wheel; therefore the traction force remains same for each wheel whether one wheel is on upper position.

Symmetric connection of two mechanisms is a critical process. Since the both sides of the bogie will work in linear part of the curve, one side will be opposite position of other side. While designing this connection we must avoid from singular configurations of the mechanism.

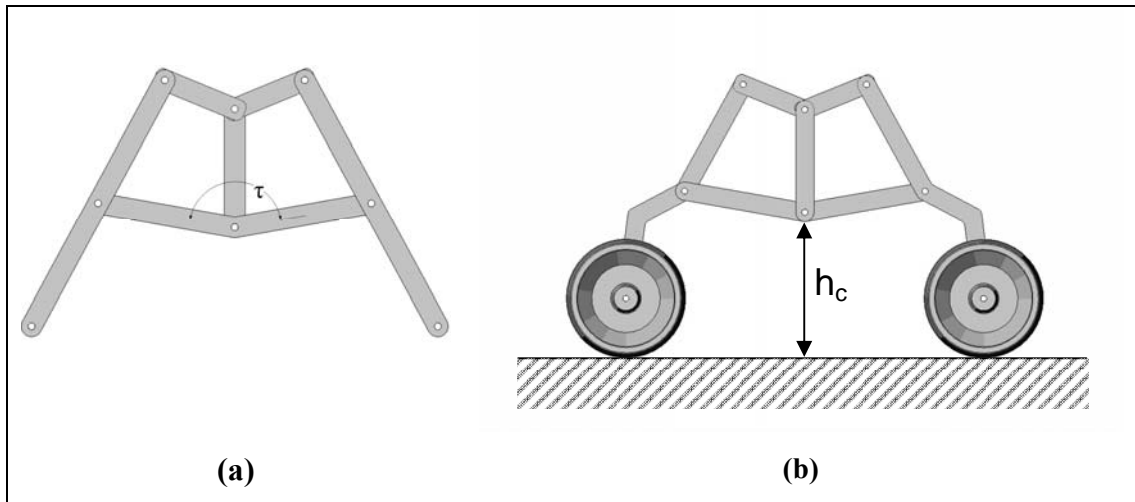


Figure 4-14: (a) Connection between two lambda mechanisms, (b) definition of ground clearance

Symmetric lambda mechanisms are connected to each other with a V-shaped rigid link. Angle τ can be selected by geometrically. The constraint of this angle is ground clearance of bogie (h_c) and maximum obstacle capacity. For our parameters, optimum connection angle $\tau = 160^\circ$.

4.2.5 Adaptation of Double-Lambda Mechanism into Rocker-Bogie

Suspension: LBS

Rocker-bogie mechanism has advantages while distributing load on the wheels nearly equal. To obtain this useful property, double lambda mechanism can be combined with former rocker-bogie design.

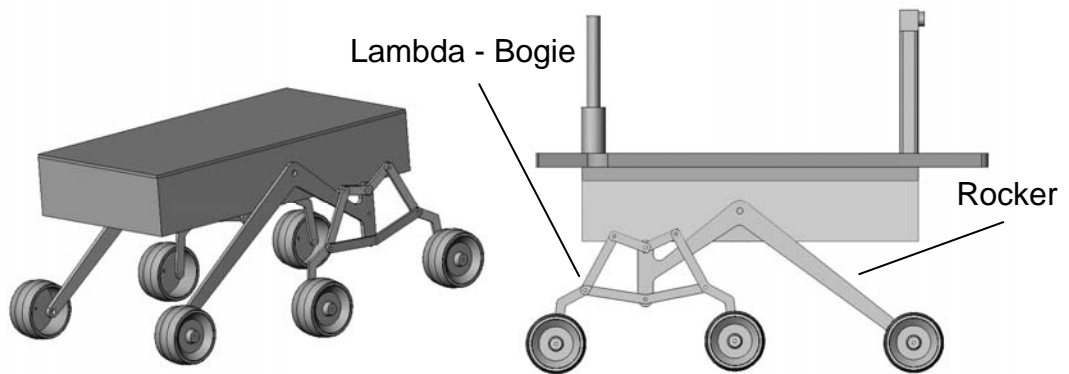


Figure 4-15: Experimental suspension design LBS

Linear Bogie Suspension (LBS) has nearly similar off-road capacity with linear bogie motion. Small angular displacement of rocker which affects linear motion of bogie can be neglected.

Two planar mechanisms are connected to each other by a differential mechanism. When one side climbing over obstacle, this mechanism rotates the main body around the rocker joints by average angle of two sides

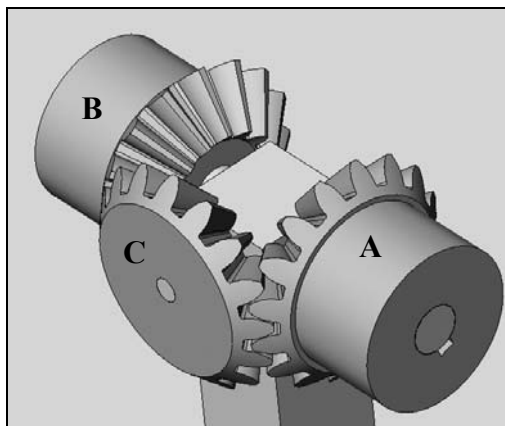


Figure 4-16: Differential gear mechanism between right and left rockers

Gear A connected to left, gear B connected to right and C is assembled on the main platform. In differential mechanisms, all gear ratios are same. That means if gear A rotates 10 degrees and gear B rotates 20 degrees, main platform will rotate 15 degrees.

4.2.6 Mobility Analysis of LBS Mechanism

Three-dimensional kinematic diagram of whole LBS mechanism is shown in figure 4-17. We can assume a cardan joint connected between two rockers instead of differential mechanism for easier calculation.

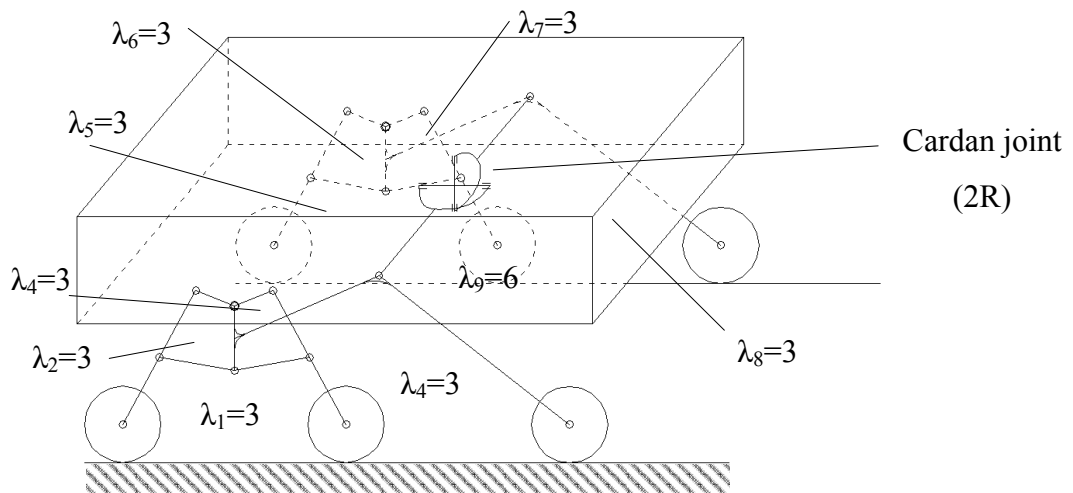


Figure 4-17: LBS kinematic diagram

Structural formula with variable general constraint for the mechanical system (4.2) is;

$$W = \sum_{i=1}^j f_i - \sum_{k=1}^L \lambda_k$$

For our mechanism;

P₁ – Kinematic pairs with one degree of freedom : 22

P₂ – Kinematic pairs with two degrees of freedom (higher kinematic pairs): 12 and 1 universal joint (with 2R)

On the left and right side of the mechanism, we have 8 loops with $\lambda = 3$ and 1 spatial mechanism (Cardan joint) $\lambda = 6$. Therefore;

$$\sum_{k=1}^L \lambda_k = \sum_{k=1}^8 3 + \sum_{k=1}^1 6 = 8 \cdot 3 + 1 \cdot 6 = 30$$

$$W = \sum_{i=1}^j f_i - \sum_{k=1}^L \lambda_k = (22 + 12 + 2) - 30 = 6$$

Mobility analysis shows that rover suspension mechanism has total 6 degrees of freedom.

4.2.7 Various Design Possibilities with Linear Motion Bogie

Adapting to terrain parameters, there are different possibilities for rover suspension like LBS. Spring and damper application to double lambda suspension good solution for high-speed off-road vehicles.

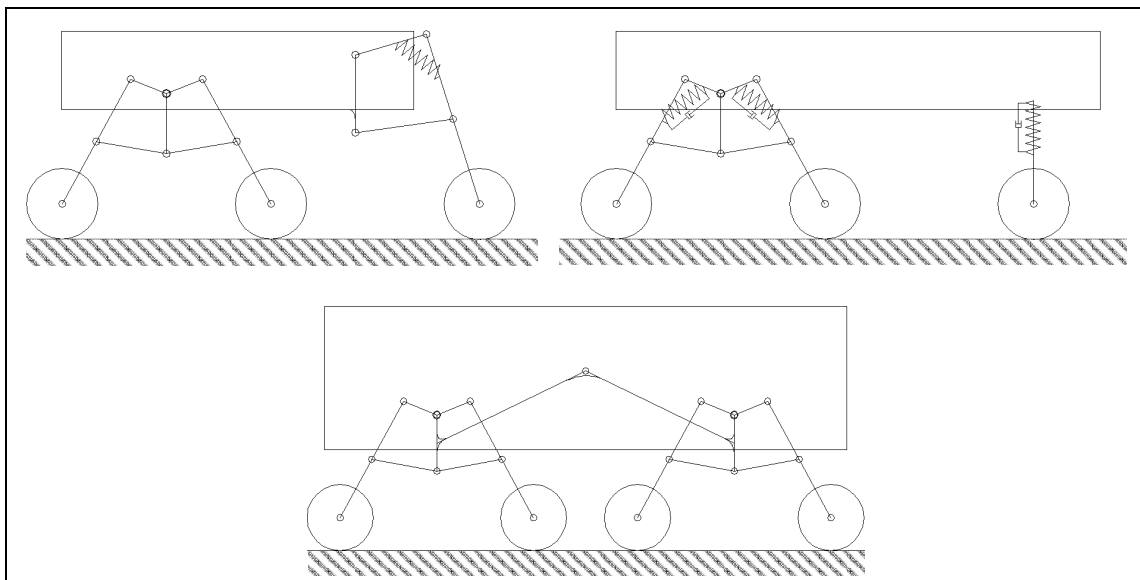


Figure 4-18: Different applications of lambda bogie suspension

Chapter 5

POSITION ANALYSIS OF LAMBDA MECHANISM

5.1. Coupler Curve Function and Trajectory of the Wheel

5.1.1 Vector Loop Equations

It is essential to determine the position and the behaviour of the tip point function P *analytically*. For this purpose, we can write vector loop equations to acquire mathematical definition of coupler point.

The resulting vector components contain two parameters which are dependent to each other named α and θ . We will assume that θ is the input angle. Thus, the other angle α can be calculated by using geometric and trigonometric relations.

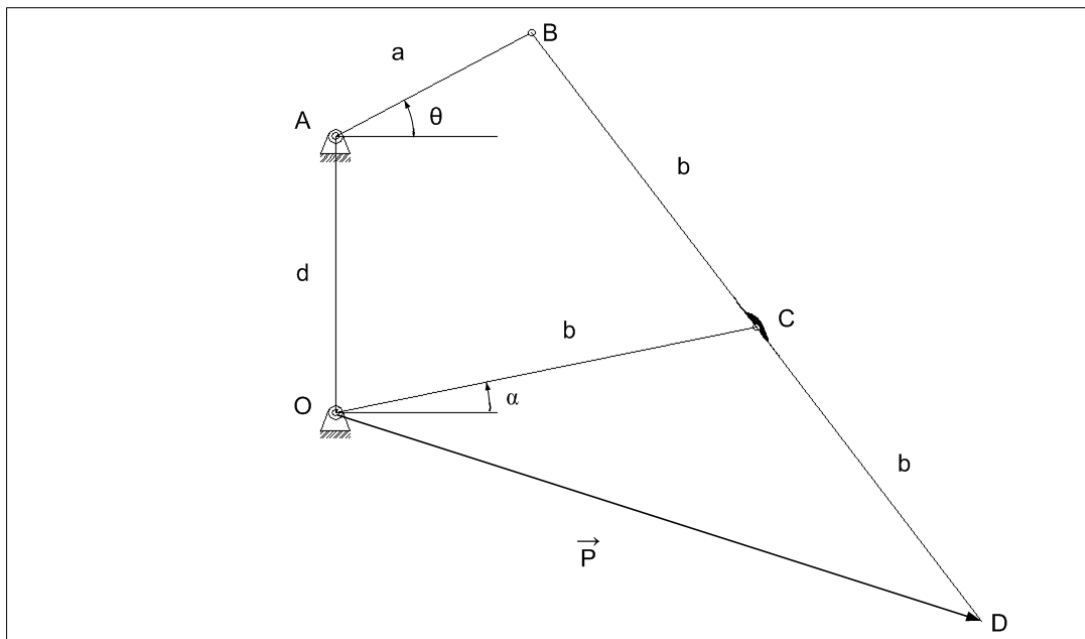


Figure 5-1: Description of position vector P

This closed curve function can be calculated by using 2 vector equations. First equation starts from the origin O, ends at B.

$$\overrightarrow{OB} = \overrightarrow{v_2} + \overrightarrow{v_3} \quad (5.1)$$

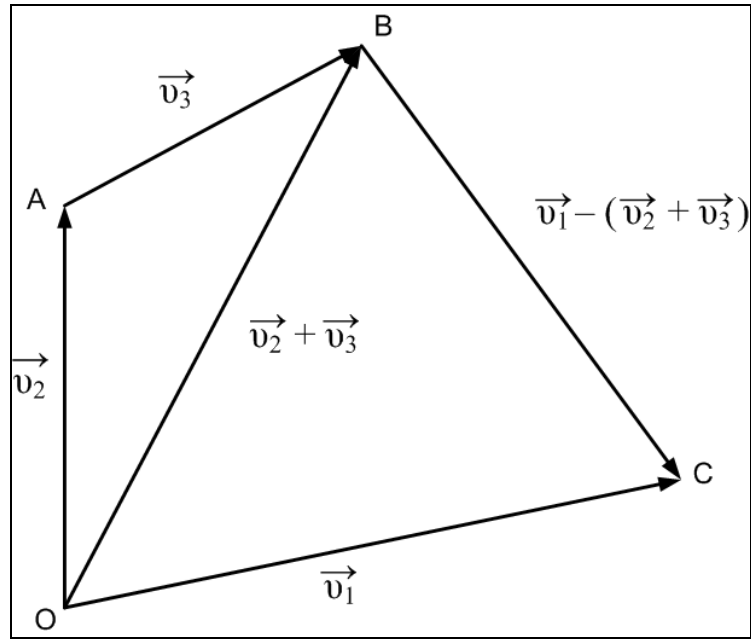


Figure 5-2: Vector loops on lambda mechanism

Second vector is located between point B and C.

$$\overrightarrow{BC} = \overrightarrow{v_1} - (\overrightarrow{v_2} + \overrightarrow{v_3}) \quad (5.2)$$

where;

$$\overrightarrow{v_1} = +b(\text{Cos}\alpha\vec{i} + \text{Sin}\alpha\vec{j}) \quad (5.3)$$

$$\overrightarrow{v_2} = +d\vec{j} \quad (5.4)$$

$$\overrightarrow{v_3} = +a(\text{Cos}\theta\vec{i} + \text{Sin}\theta\vec{j}) \quad (5.5)$$

From equation and figure 5-2, vector **P** can be calculated as;

$$\vec{P} = \overrightarrow{v_1} + (\overrightarrow{v_1} - (\overrightarrow{v_2} + \overrightarrow{v_3})) \quad (5.6)$$

If we put equation (5.3), (5.4) and (5.5) into equation (5.2);

$$\begin{aligned} \vec{P} &= 2b(\text{Cos}\alpha\vec{i} + \text{Sin}\alpha\vec{j}) - d\vec{j} - a(\text{Cos}\theta\vec{i} + \text{Sin}\theta\vec{j}) \\ \vec{P} &= (2b\text{Cos}\alpha - a\text{Cos}\theta)\vec{i} + (2b\text{Sin}\alpha - d - a\text{Sin}\theta)\vec{j} \end{aligned} \quad (5.7)$$

Cartesian components of this vector function can be divided into parts;

$$\vec{P}_x = 2b\cos\alpha - a\cos\theta \quad (5.8)$$

$$\vec{P}_y = 2b\sin\alpha - d - a\sin\theta \quad (5.9)$$

5.1.2 Angular Relations

It can be seen from (5.8) and (5.9), we need two parameters to determine coupler curve. Since the mechanism is 1 DOF, we can find an equation between α and θ from geometric relations.

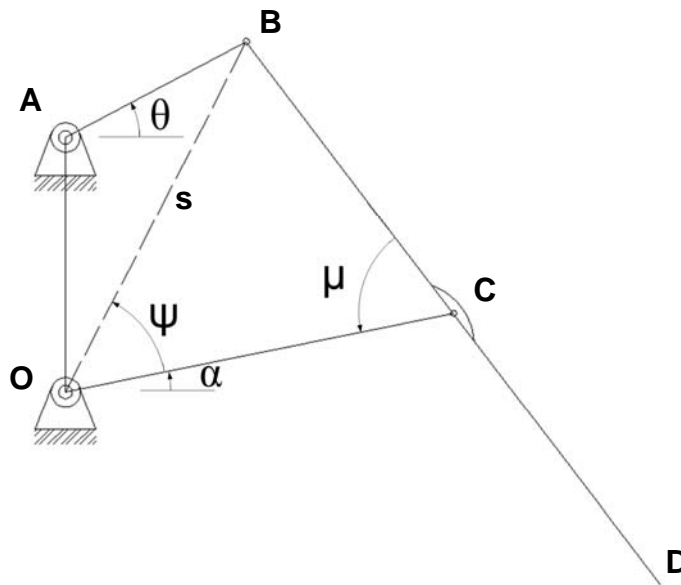


Figure 5-3: Angles between linkages

Let us write cartesian components of point B;

$$x_B = s\cos\theta = a\cos\theta \quad (5.10)$$

$$y_B = s\sin\theta = a\sin\theta + d \quad (5.11)$$

OB distance;

$$S = \sqrt{x_B^2 + y_B^2} \quad (5.12)$$

Angular position of AB link becomes;

$$\phi = a \tan 2(x_B, y_B) \quad (5.13)$$

$$\mu = \pm \text{Cos}^{-1} \left[\frac{h^2 + b^2 - s^2}{2hb} \right] = \pm \text{Cos}^{-1} \left[\frac{2b^2 - s^2}{2b^2} \right] \quad (5.14)$$

by the same manner with equation 5.14;

$$\Psi = \pm \text{Cos}^{-1} \left[\frac{b^2 + s^2 - h^2}{2bs} \right] = \pm \text{Cos}^{-1} \left[\frac{b^2 + s^2 - b^2}{2bs} \right] = \pm \text{Cos}^{-1} \left[\frac{s^2}{2bs} \right] \quad (5.15)$$

$$\alpha = \phi - \Psi \quad (5.16)$$

We can calculate all angles relative to input angle θ by using these relations.

5.1.3 Coupler Curve Function

We can draw P vector's different positions relative to an input angle by using equation (5.8) and (5.9). Coupler curve function has two parameters α and θ , which are dependent to each other.

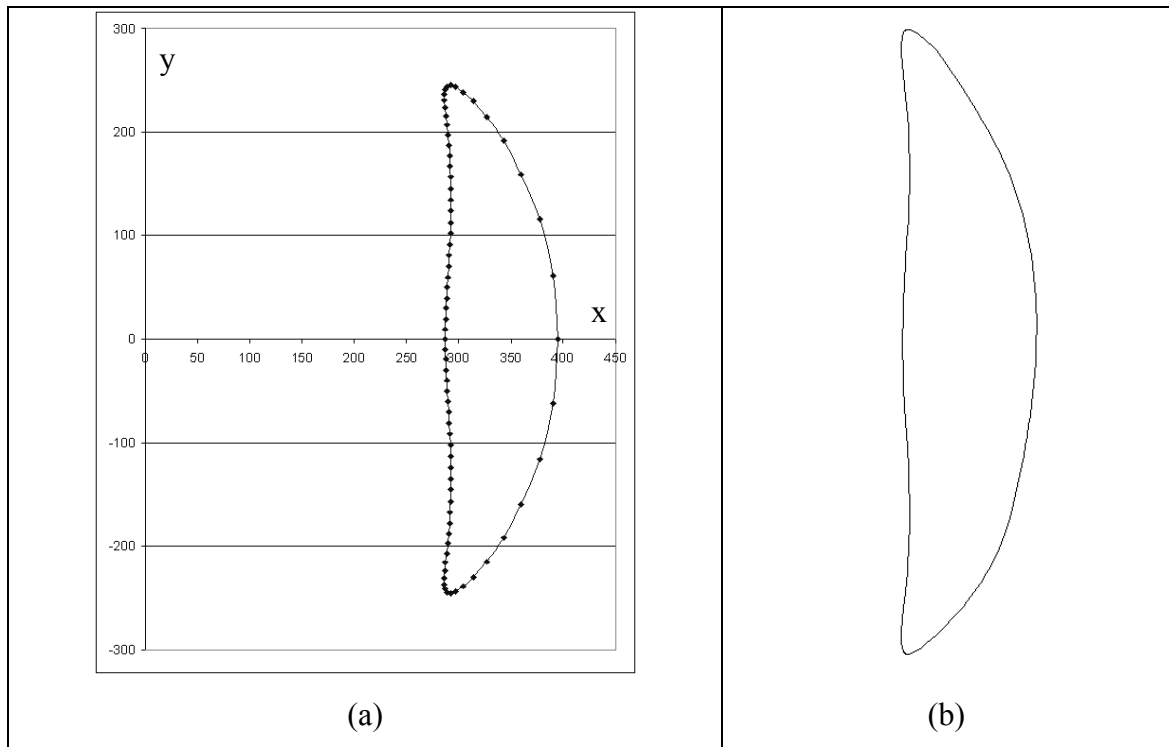


Figure 5-4: Graph of function P (a) and geometrical trajectory (b)

Figure 5.4a is graphical representation of (5.8) and (5.9). As we can see in figure 5.4b, it fits exactly with geometrical trajectory. Small deviations from ideal line can also be seen which has discussed by Chebyshev. Maximum error is approximately 1% of total y-axis motion, which can be neglected. The linear part of this curve is parallel to the base frame.

5.2 Singularity Analysis

5.2.1 Singular Configurations Relative to α

For singularity analysis we have to obtain input angle relative to transmission angle. In lambda mechanism, transmission angle is shown in figure 5-5;

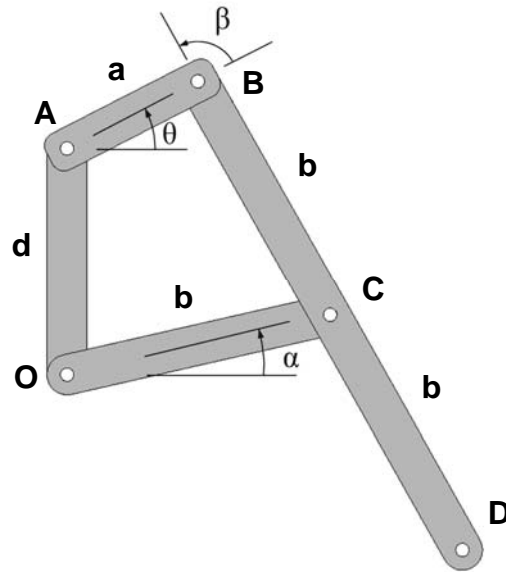


Figure 5-5: Transmission angle

If β goes to zero, mechanism will reach first singularity. Let us derive a function between transmission angle β and OC link;

We can write a vector loop equation of point B;

$$\vec{OA} + \vec{AB} = \vec{OC} + \vec{CB} \quad (5.17)$$

x components :

$$a \cos \theta = b \cos \alpha + b \cos(\theta + \beta) \quad (5.18)$$

y components:

$$d + a \sin \theta = b \sin \alpha + b \sin(\theta + \beta) \quad (5.19)$$

Since our aim is to calculate angle α relative to angle β , θ has to be excluded from this equation. For this purpose, all terms which include θ are left on right hand side of (5.18) and (5.19).

$$-b \cos \alpha = -a \cos \theta + b \cos(\theta + \beta) \quad (5.20)$$

$$-b \sin \alpha + d = -a \sin \theta + b \sin(\theta + \beta) \quad (5.21)$$

If we take square of both equations and add them;

$$b^2 + d^2 - 2bd\sin\alpha = a^2 + b^2 - 2ab\cos(\theta + \beta) - 2ab\sin\theta \cdot \sin(\theta + \beta)$$

$$b^2 + d^2 - 2bd\sin\alpha = a^2 + b^2 - 2ab\cos\beta$$

that gives;

$$\sin\alpha = \frac{d^2 - a^2 + 2ab\cos\beta}{2bd} \quad (5.22)$$

As we know from trigonometric relations;

$$\cos\beta = \pm\sqrt{1 - \sin^2\beta} \quad (5.23)$$

to reach a solution β must be double root as 0 and π radians.

Physically meaning of this condition is that, singularity occurs if transmission angle 0 or 180 degrees. In this configuration crank cannot transmit force.

Calculation of 5.22 with our construction parameters;

$$a = 109 \text{ mm}$$

$$b = 200 \text{ mm}$$

$$d = 169 \text{ mm}$$

yields;

First singularity ($\beta = 0^\circ$) occurs at $\alpha = 63.089674^\circ$

Second singularity ($\beta = 180^\circ$) occurs at $\alpha = 336.532747^\circ$

Both results exactly fit with geometric results.

5.2.2 Singular Configurations Relative to θ

We can also calculate singular configurations relative to θ angle. By using same vector loop of (5.17);

$$\vec{OA} + \vec{AB} = \vec{OC} + \vec{CB}$$

x components :

$$a\cos\theta = b\cos\alpha + b\cos(\theta + \beta)$$

y components:

$$d + a\sin\theta = b\sin\alpha + b\sin(\theta + \beta)$$

to exclude α term we can re-arrange these equations;

$$a\cos\theta - b\cos(\theta + \beta) = b\cos\alpha \quad (5.24)$$

$$a\sin\theta - b\sin(\theta + \beta) + d = b\sin\alpha \quad (5.25)$$

Adding the squares of both sides;

$$\begin{aligned} a^2\cos^2\theta + b^2\cos^2(\theta + \beta) - 2ab\cos\theta\cos(\theta + \beta) + a^2\sin^2\theta + b^2\sin^2(\theta + \beta) + d^2 \\ - 2ab\sin\theta\sin(\theta + \beta) - 2bd\sin(\theta + \beta) + 2ad\sin\theta = b^2 \end{aligned}$$

$$\begin{aligned} a^2 + b^2 + d^2 - 2ab\cos\theta\cos(\theta + \beta) - 2ab\sin\theta\sin(\theta + \beta) \\ - 2bd\sin(\theta + \beta) + 2ad\sin\theta = b^2 \end{aligned} \quad (5.26)$$

and arranging Sine and Cosine terms;

$$\begin{aligned} a^2 + d^2 - 2ab\cos\theta(\cos\theta\cos\beta - \sin\theta\sin\beta) - 2ab\sin\theta(\sin\theta\cos\beta + \sin\beta\cos\theta) \\ - 2bd(\sin\theta\cos\beta + \sin\beta\cos\theta) + 2ad\sin\theta = 0 \end{aligned} \quad (5.27)$$

If we apply angle-sum formula;

$$\begin{aligned} a^2 + d^2 - 2ab\cos^2\theta\cos\beta + 2ab\cos\theta\sin\theta\sin\beta - 2ab\sin^2\theta\cos\beta - 2ab\sin\theta\sin\beta\cos\theta \\ - 2bd\sin\theta\cos\beta - 2bd\sin\beta\cos\theta + 2ad\sin\theta = 0 \end{aligned} \quad (5.28)$$

$$a^2 + d^2 - 2ab\cos\beta - 2bd\sin\theta\cos\beta - 2bd\sin\beta\cos\theta + 2ad\sin\theta = 0 \quad (5.29)$$

This equation can be shortened as;

$$A(\beta) \cdot \cos\theta + B(\beta) \cdot \sin\theta + C(\beta) = 0 \quad (5.30)$$

where

$$A(\beta) = -2bd\sin\beta \quad (5.31)$$

$$B(\beta) = 2ad - 2bd\cos\beta \quad (5.32)$$

$$C(\beta) = a^2 + d^2 - 2ab\cos\beta \quad (5.33)$$

Solution of constraint equation (5.30)

$$\theta = 2 \tan^{-1} \left(\frac{-B \pm \sqrt{B^2 - (C^2 - A^2)}}{C - A} \right) \quad (5.34)$$

Calculation of 5.34 with our construction parameters;

First singularity ($\beta = 0^\circ$) occurs at $\theta = 185.893084^\circ$

Second singularity ($\beta = 180^\circ$) occurs at $\theta = 306.420997^\circ$

5.3 Symmetric Side Inverse Position Analysis

By using (5.15) and (5.16), we can find angular position of mechanism relative to θ . On the opposite side of the mechanism, input becomes α angle. For this reason, we need to find a relation between output angle α and input angle θ to make inverse position analysis.

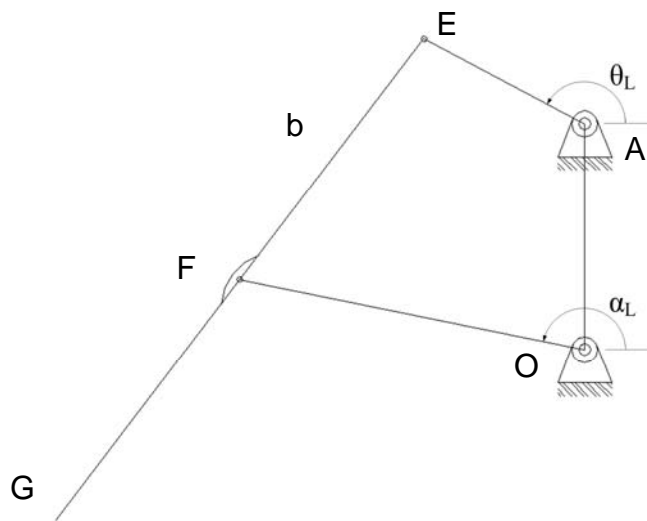


Figure 5-6: Left side of the bogie mechanism

Due to the distance b , between E and F will remain fixed, we can write the following equation;

$$(\mathbf{F} - \mathbf{E}) \cdot (\mathbf{F} - \mathbf{E}) - b^2 = 0 \quad (5.35)$$

The coordinates of point F and E are;

$$\mathbf{E} = \begin{Bmatrix} a \cos \theta \\ a \sin \theta \end{Bmatrix} \text{ and } \mathbf{F} = \begin{Bmatrix} b \cos \alpha \\ -d + b \sin \alpha \end{Bmatrix} \quad (5.36)$$

$$b^2 \cos^2 \alpha + a^2 \cos^2 \theta - 2ba \cos \alpha \cos \theta + d^2 + b^2 \sin^2 \alpha + a^2 \sin^2 \theta - 2db \sin \alpha - 2ab \sin \alpha \sin \theta + 2ad \sin \theta - b^2 = 0 \quad (5.37)$$

$$(-2ba \cos \alpha) \cos \theta + (2ad - 2ab \sin \alpha) \sin \theta - 2db \sin \alpha + b^2 + a^2 + d^2 - b^2 = 0$$

$$A(\alpha) \cos \theta + B(\alpha) \sin \theta = C(\alpha) \quad (5.38)$$

where,

$$A(\alpha) = -2ba \cos \alpha$$

$$B(\alpha) = 2ad - 2ab \sin \alpha$$

$$C(\alpha) = -2db \sin \alpha + a^2 + d^2$$

Solution of this constraint function has been discussed in Appendix B;

$$\theta(\alpha) = \arctan\left(\frac{B}{A}\right) \pm \arccos\left(\frac{C}{\sqrt{A^2 + B^2}}\right) \quad (5.39)$$

5.4 Singular Positions of Double-Lambda Bogie Mechanism

The double lambda connection restricts the motion of each side. That means one of the singularities is not inside the workspace. For our mechanism, first singularity stays out of range.

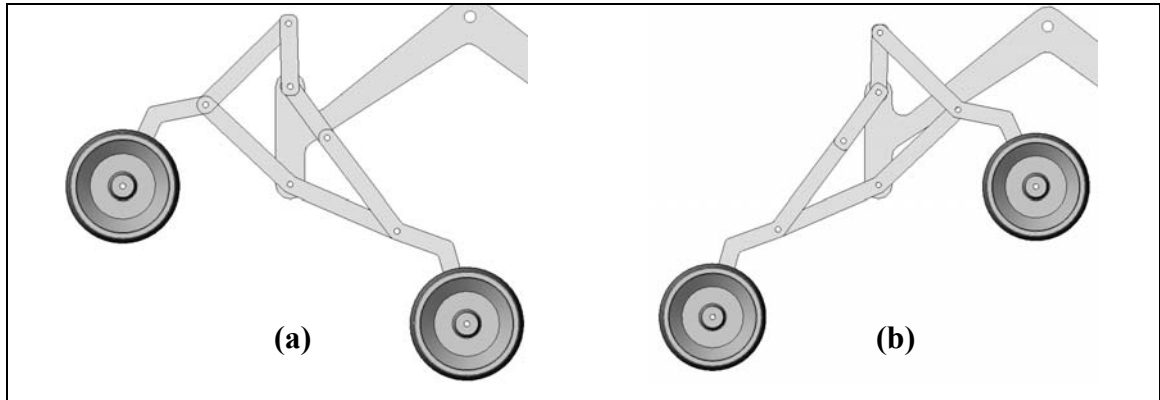


Figure 5-7: Singular configurations of right (a) and left (b) side of the bogie

Angular positions of each side where singularity occurs;

Second singularity ($\beta = 180^\circ$) of *right side*

$$\theta_R = 306.42^\circ, \theta_L = 91.91^\circ$$

Second singularity ($\beta = 180^\circ$) of *left side*

$$\theta_L = 233.58^\circ, \theta_R = 88.09^\circ$$

First singularity is not possible for bogie mechanism since this configuration is out of range. For safety, we must avoid from second singular positions with a safety margin angle (i.e. 10 degrees) on both sides. A stopper can be used for this purpose.

Chapter 6

STATIC ANALYSIS

6.1 Wheel Reaction Forces

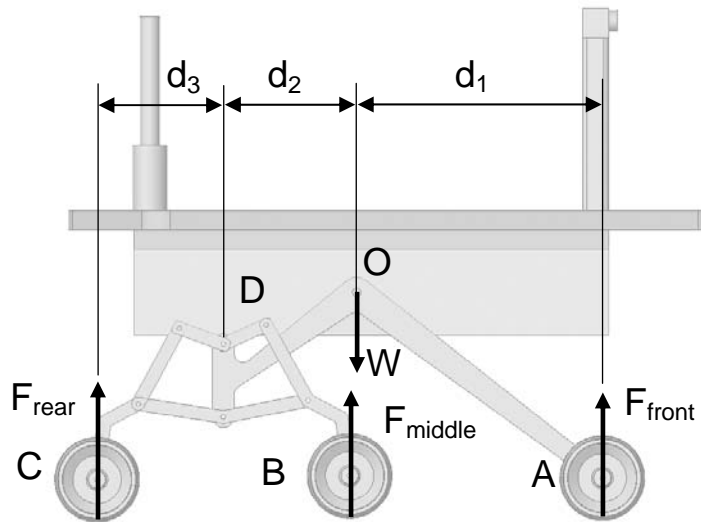


Figure 6-1: Force diagram of LBS

If bogie is symmetrical, distances between CD and DB will be equal. For this reason, reaction forces of rear and middle wheels are the identical.

Moment on point O;

$$M_o = (F_{rear} + F_{middle}) \cdot d_2 - F_{front} \cdot d_1 \quad (6.1)$$

For equilibrium;

$$M_o = 0$$

$$(F_{rear} + F_{middle}) \cdot d_2 = F_{front} \cdot d_1 \quad (6.2)$$

If $\frac{d_2}{d_1} = \frac{1}{2}$, the reaction forces will be equal. Due to fact that, for small angular displacements horizontal displacements will be very small, reaction forces will be very close to each other. For our design, $\frac{d_2}{d_1} = 0.75$ to increase climbing capacity.

6.2 Stability Definition of a Mobile Robot

During operation on rough terrain, another problem is stability of the rover. If a robot can maintain its balance at all time in freezing position, it can be said that the robot has static stability. Physically, the boundary for stability criteria is related with polygon, which consists of contact points of wheels and ground [3].

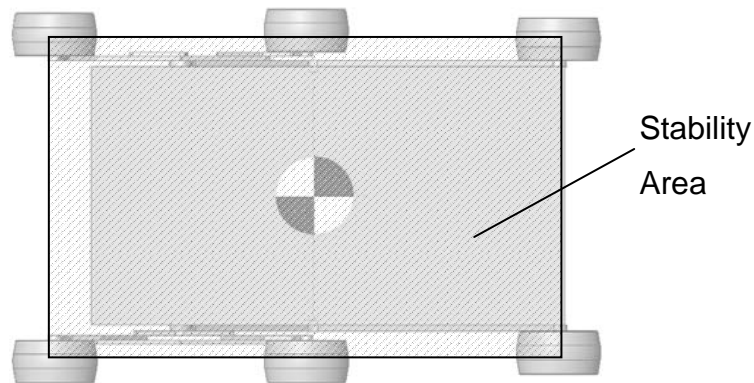


Figure 6-2: Stability area consists of contact points

If center of gravity projection on the ground plane, stays inside of the stability area robot will be stable. This shape can be narrowed depending on safety factor. The stability of robot, which is stationary or moving with constant speed, can be defined with gravitational stability margin [26]. This margin is the minimum distance between projection of center of gravity on the ground plane to the edge of convex region.

The maximum slope of the terrain where robot can climb is called gradeability. Maximum downhill and cross-hill gradeability definitions are:

6.2.1 Down-Hill Gradeability

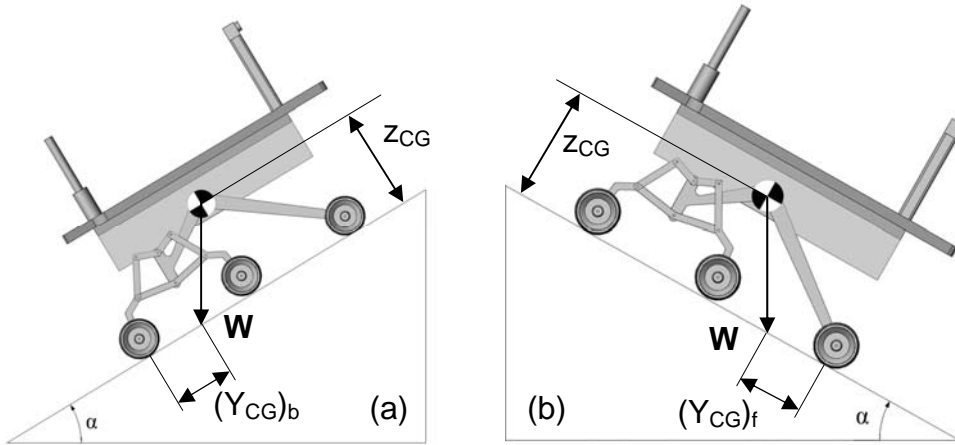


Figure 6-3: Downhill rear (a) and front (b) stability margins and dimensions

$$\alpha_{d\max} = \min \left\{ \arctan \left(\frac{(Y_{CG})_f}{z_{CG}} \right), \arctan \left(\frac{(Y_{CG})_b}{z_{CG}} \right) \right\} \quad (6.3)$$

6.2.2 Cross-hill Gradeability

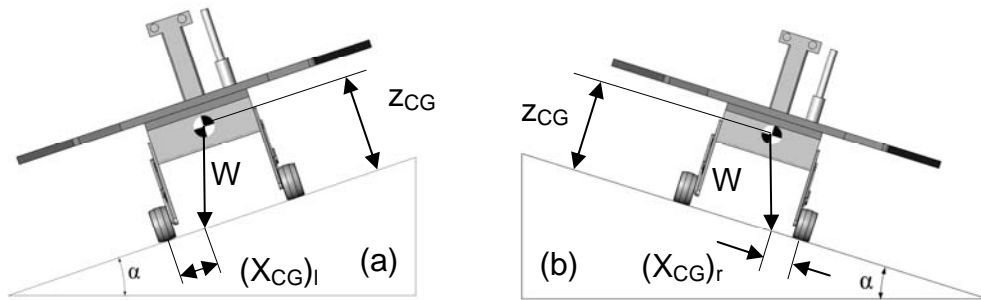


Figure 6-4: Lateral stability margins and dimensions

$$\alpha_{c\max} = \min \left\{ \arctan \left(\frac{(X_{CG})_l}{z_{CG}} \right), \arctan \left(\frac{(X_{CG})_r}{z_{CG}} \right) \right\} \quad (6.4)$$

The maximum slope and stability margins can be calculated by;

$$Y_{CG} \geq z_{CG} \tan \alpha_{d\max} (1 + SM) \quad (6.5)$$

$$B_{WW} \geq z_{CG} \tan \alpha_{d\max} (1 + SM) \quad (6.6)$$

In equation (6.5) and (6.6), term SM is called safety margin which is a safety factor for uncertainties of wheel and center of gravity position.

Values for LBS are;

$$Z_{CG} = 490 \text{ mm}$$

$$L_{WW} = 1172 \text{ mm}$$

$$B_{WW} = 760 \text{ mm}$$

For SM = 1, limit angles can be calculated as;

$$\text{Front downhill gradeability, } \alpha_{dmax} = 45.58^\circ$$

$$\text{Rear downhill gradeability, } \alpha_{dmax} = 53.90^\circ$$

$$\text{Right – Left cross-hill gradeability, } \alpha_{dmax} = 37.79^\circ$$

Chapter 7

EQUATION OF MOTION

7.1 Second Order Lagrange Equation

For a mechanism with several degrees of freedom, the equation of motion usually described by second order Lagrange equation;

$$\frac{d}{dt} \left(\frac{\partial T}{\partial \dot{q}_i} \right) - \frac{\partial T}{\partial q_i} = Q_i, \quad i = 1, 2, \dots, s \quad (7.1)$$

where T is kinetic energy of system, i is number of input coordinates, which has equal degree of freedoms, q_i input coordinates, Q_i equivalent forces.

Equivalent forces Q_i are defined from condition of equality elementary works of its forces on virtual displacements coinciding with variety of input coordinates to the works of external forces applying to the links of the mechanism on its virtual locations;

$$\sum_{i=1}^s Q_i \delta q_i = \sum_{j=1}^m (F_{jx} \delta x_j + F_{jy} \delta y_j + F_{jz} \delta z_j + M_{jx} \delta \varphi_j + M_{jy} \delta \gamma_j + M_{jz} \delta \psi_j) \quad (7.2)$$

where

F_{jx}, F_{jy}, F_{jz} - components of external forces \mathbf{F}_j

M_{jx}, M_{jy}, M_{jz} - components of external moments \mathbf{M}_j

$\delta x_j, \delta y_j, \delta z_j$ - virtual translational displacements of the points of acting external forces

$\delta \varphi_j, \delta \gamma_j, \delta \psi_j$ - virtual rotational displacements of the lines at applying external moments

Usually the elementary work of the all external forces are defined step by step by changing just one input coordinate on fixed the others input coordinates.

Thus,

$$\begin{aligned}\delta x_j &= \frac{\partial x_j}{\partial q_i} \delta q_i, \quad \delta y_j = \frac{\partial y_j}{\partial q_i} \delta q_i, \quad \delta z_j = \frac{\partial z_j}{\partial q_i} \delta q_i \\ \delta \varphi_j &= \frac{\partial \varphi_j}{\partial q_i} \delta q_i, \quad \delta \gamma_j = \frac{\partial \gamma_j}{\partial q_i} \delta q_i, \quad \delta \psi_j = \frac{\partial \psi_j}{\partial q_i} \delta q_i\end{aligned}\quad (7.3)$$

using equations (7.2) and (7.3), the expression, equivalent forces and moments can be shown as;

$$Q_i = \sum_{j=1}^m \left(F_{jx} \frac{\partial x_j}{\partial q_i} + F_{jy} \frac{\partial y_j}{\partial q_i} + F_{jz} \frac{\partial z_j}{\partial q_i} + M_{jx} \frac{\partial \varphi_j}{\partial q_i} + M_{jy} \frac{\partial \gamma_j}{\partial q_i} + M_{jz} \frac{\partial \psi_j}{\partial q_i} \right) \quad (7.4)$$

The gravity and elasticity forces are into account by changing the potential energy of the mechanical system. Then the Lagrange motion equation (7.1) can be written in the following form;

$$\frac{d}{dt} \left(\frac{\partial T}{\partial \dot{q}_i} \right) - \frac{d}{dt} \left(\frac{\partial \Pi}{\partial \dot{q}_i} \right) - \frac{\partial T}{\partial q_i} + \frac{\partial \Pi}{\partial q_i} = Q_i$$

$$\text{or } \frac{d}{dt} \frac{\partial(T - \Pi)}{\partial \dot{q}_i} - \frac{\partial(T - \Pi)}{\partial q_i} = Q_i$$

$$\text{or } \frac{d}{dt} \frac{\partial L}{\partial \dot{q}_i} - \frac{\partial L}{\partial q_i} = Q_i \quad (7.5)$$

where $L = T - \Pi$ called Lagrange function.

Friction forces and moments are considered in Lagrange motion equation (7.5) for cases only when they don't depend on reaction forces of kinematic pairs. In that case, friction forces can be included in expression of equivalent forces (7.2). In vibration analysis, the friction forces can be taken into account as force which is proportional to input velocity \dot{q}_i and introduced as dissipative function of Releia;

$$\Phi = \frac{1}{2} \sum_{i=1}^s \sum_{j=1}^s b_{ij} \dot{q}_i \dot{q}_j \quad (7.6)$$

where b_{ij} is a constant coefficient.

Using equation (7.6) and Lagrange motion equation (7.5), we can describe in the general form second order of motion equation of a mechanical system with several degree of freedom by taking into account kinetic and potential energies and dissipative function as;

$$\frac{d}{dt} \frac{\partial L}{\partial \dot{q}_i} - \frac{\partial \Phi}{\partial \dot{q}_i} + \frac{\partial L}{\partial q_i} = Q_i \quad , i = 1, \dots, s \quad (7.7)$$

If the input coordinate q_i is cycle coordinate, the Lagrange equation (7.7) can be integrated with respect to cycle coordinate.

7.2 Motion of Rover Suspension Mechanism

The rover suspension mechanism LBS consist of two symmetrical mechanisms on right and left sides of the rover body with six actuated wheels. Equation of motion which describe the left side motion, will be valid for the right side mechanism. When rover moving on even surface, all links of the mechanism will move parallel with respect to fixed coordinates.

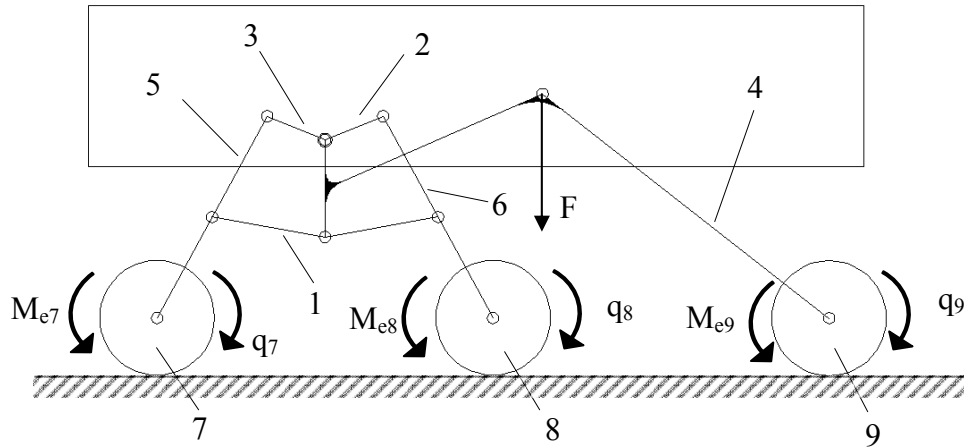


Figure 7-1: Equivalent forces and virtual displacements of LBS

The structural formula to calculate the mobility for moving frame at rover suspension mechanism for one side can be described as;

$$q = W - f_l - 2f_h + \sum_{k=1}^L \lambda_k \quad (7.8)$$

where $W=3$, $f_l = 11$, $f_h = 3$, $L = 5$ that gives; $q = 1$

Using formula (7.8) also for the right side, we get $q = 1$

The first position of rover suspension mechanism as shown in *figure 7.2* wheel numbered 7 while climbing over obstacle. This motion changes the position of mechanism by link 5. As the input angle q_7 and equivalent moment, M_{e7} will be applied to actuator 7, which will move up by driving forces P_{d7} .

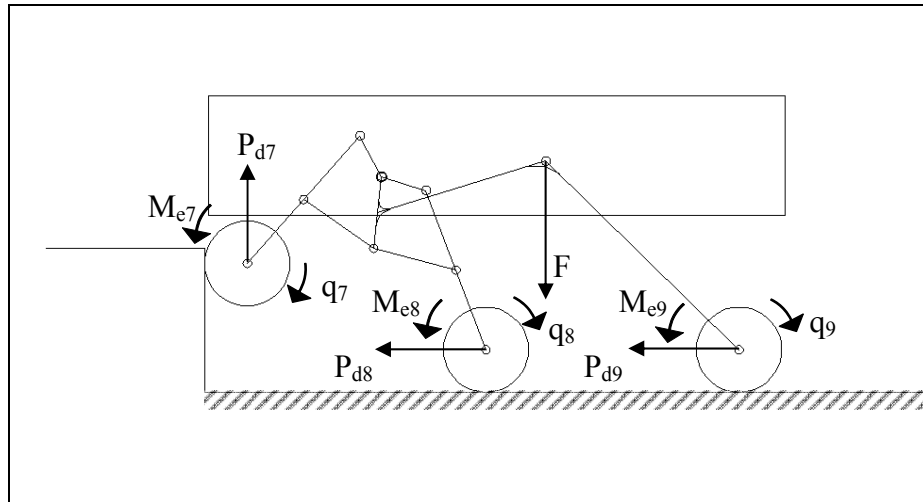


Figure 7-2: Reverse step climbing first configuration

The second position of rover suspension mechanism as shown in *figure 7.3*, wheel 8 climbs and linkage mechanism change its position and equivalent moment M_{e8} . Wheel 8 will move up with force P_{d8} .

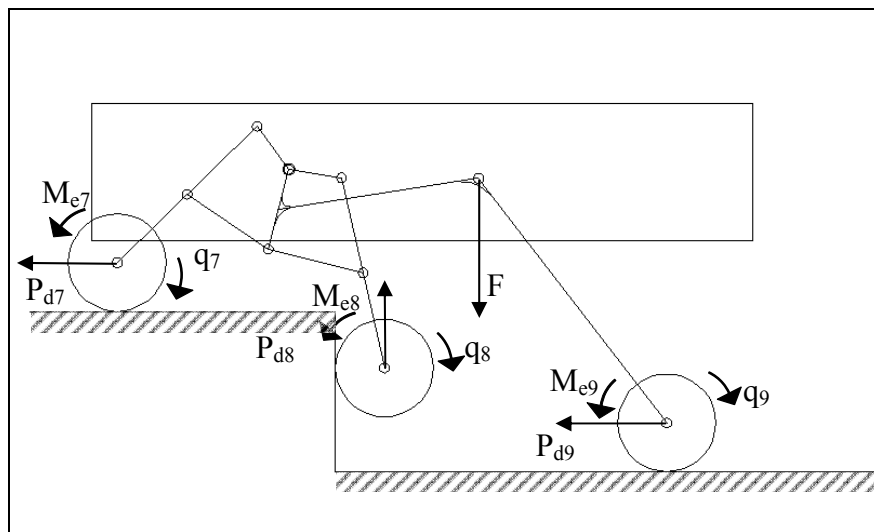


Figure 7-3: Reverse step climbing second configuration

The third position is shown in *figure 7.4*. For this configuration, input angle q_9 and equivalent moment M_{e9} applying to wheel 9 will move the linkage mechanism by link 4 and active driving force P_{d9} .

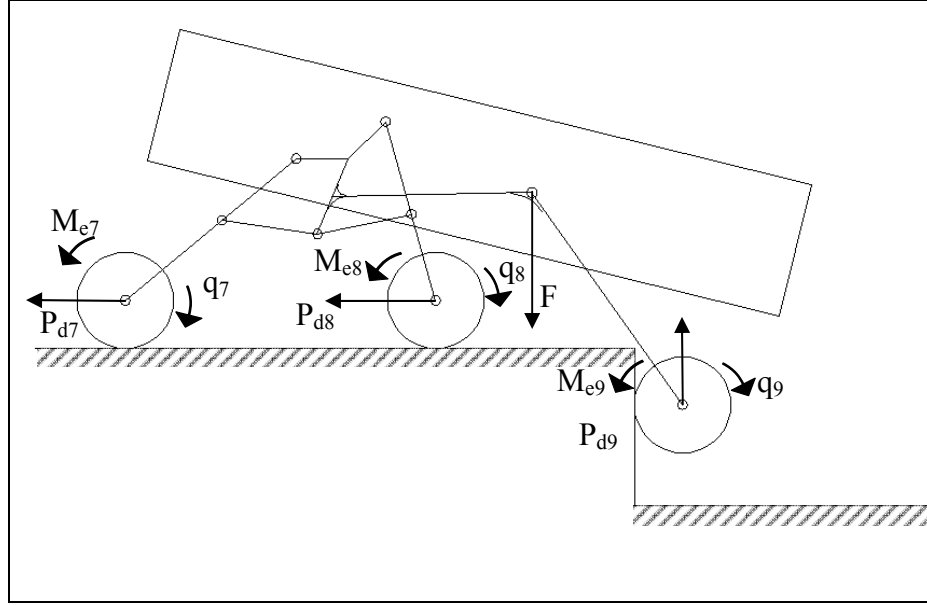


Figure 7-4: Reverse step climbing third configuration

7.3 Equation of Motion of Linkage Mechanism with Three Degrees of Freedom

Assuming input rotations q_7 , q_8 and q_9 of actuators on wheels numbered 7, 8 and 9 respectively, we can write the following Lagrange equations;

$$\frac{d}{dt} \frac{\partial T}{\partial \dot{q}_7} - \frac{\partial T}{\partial q_7} = M_{e7}$$

$$\frac{d}{dt} \frac{\partial T}{\partial \dot{q}_8} - \frac{\partial T}{\partial q_8} = M_{e8}$$

$$\frac{d}{dt} \frac{\partial T}{\partial \dot{q}_9} - \frac{\partial T}{\partial q_9} = M_{e9}$$

where M_{e7} , M_{e8} and M_{e9} are equivalent moments of forces

Kinetic energy of mobile vehicle T can be defined by assuming that links 1, 2, 3 and 4 are in balance and mass effects at link 5 and 6 neglecting,

$$T = \frac{1}{2} (I_7 \omega_7^2 + I_8 \omega_8^2 + I_9 \omega_9^2 + I_1 \omega_1^2 + I_2 \omega_2^2 + I_3 \omega_3^2 + I_4 \omega_4^2) \quad (7.9)$$

where;

$I_1, I_2, I_3, I_4, I_7, I_8, I_9$ - moment of inertia of links

1, 2, 3, 4, 7, 8 and 9 with respect to rotation axis

$\omega_1, \omega_2, \omega_3, \omega_4, \omega_7, \omega_8$ and ω_9 –angular velocities of links 1, 2, 3, 4, 7, 8 and 9

The rotation angles $\varphi_1, \varphi_2, \varphi_3$ and φ_4 at links 1, 2, 3 and 4 are functions of rotation input angles φ_7, φ_8 and φ_9 at input links 7, 8 and 9 respectively.

$$\begin{aligned}\varphi_1 &= \varphi_1(\varphi_7, \varphi_8, \varphi_9) \quad , \quad \varphi_2 = \varphi_2(\varphi_7, \varphi_8, \varphi_9) \\ \varphi_3 &= \varphi_3(\varphi_7, \varphi_8, \varphi_9) \quad , \quad \varphi_4 = \varphi_4(\varphi_7, \varphi_8, \varphi_9)\end{aligned}\tag{7.10}$$

Time derivation of equation (7.10) gives angular velocities $\tilde{\omega}_1, \tilde{\omega}_2, \tilde{\omega}_3$ and $\tilde{\omega}_4$;

$$\begin{bmatrix} \tilde{\omega}_1 \\ \tilde{\omega}_2 \\ \tilde{\omega}_3 \\ \tilde{\omega}_4 \end{bmatrix} = \begin{bmatrix} \frac{\partial \varphi_1}{\partial \varphi_7} & \frac{\partial \varphi_1}{\partial \varphi_8} & \frac{\partial \varphi_1}{\partial \varphi_9} & 0 \\ \frac{\partial \varphi_2}{\partial \varphi_7} & \frac{\partial \varphi_2}{\partial \varphi_8} & \frac{\partial \varphi_2}{\partial \varphi_9} & 0 \\ \frac{\partial \varphi_3}{\partial \varphi_7} & \frac{\partial \varphi_3}{\partial \varphi_8} & \frac{\partial \varphi_3}{\partial \varphi_9} & 0 \\ \frac{\partial \varphi_4}{\partial \varphi_7} & \frac{\partial \varphi_4}{\partial \varphi_8} & \frac{\partial \varphi_4}{\partial \varphi_9} & 0 \end{bmatrix} \begin{bmatrix} \tilde{\omega}_7 \\ \tilde{\omega}_8 \\ \tilde{\omega}_9 \\ 0 \end{bmatrix}\tag{7.11}$$

Partial derivatives $\frac{\partial \varphi_j}{\partial \varphi_i}$, $j = 1, 2, 3, 4$ and $i = 7, 8, 9$ are transmission ratios from

links 1, 2, 3 and 4 to input links 7, 8 and 9 respectively. The matrix with partial derivatives in (7.11) is also called Jacobian matrix.

Let we describe the partial derivatives as transmission ratio coefficients:

$$u_{17}^{89} = \frac{\partial \varphi_1}{\partial \varphi_7} \quad , \quad u_{18}^{79} = \frac{\partial \varphi_1}{\partial \varphi_8} \quad , \quad u_{19}^{78} = \frac{\partial \varphi_1}{\partial \varphi_9}$$

$$\begin{aligned}
u_{27}^{89} &= \partial\varphi_2/\partial\varphi_7, \quad u_{28}^{79} = \partial\varphi_2/\partial\varphi_8, \quad u_{29}^{78} = \partial\varphi_2/\partial\varphi_9 \\
u_{37}^{89} &= \partial\varphi_3/\partial\varphi_7, \quad u_{28}^{79} = \partial\varphi_3/\partial\varphi_8, \quad u_{39}^{78} = \partial\varphi_3/\partial\varphi_9 \\
u_{47}^{89} &= \partial\varphi_4/\partial\varphi_7, \quad u_{48}^{79} = \partial\varphi_4/\partial\varphi_8, \quad u_{49}^{78} = \partial\varphi_4/\partial\varphi_9
\end{aligned} \tag{7.12}$$

where superscripts describe fixed input angles and subscripts show variable transmission ratio between output and input (e.g. transmission angle ratio u_{47}^{89} is partial derivation function of output φ_4 with input φ_7 when other input angles 8 and 9 are fixed)

The equation of (7.11) can be written as:

$$\begin{bmatrix} \tilde{\omega}_1 \\ \tilde{\omega}_2 \\ \tilde{\omega}_3 \\ \tilde{\omega}_4 \end{bmatrix} = \begin{bmatrix} u_{17}^{89} & u_{18}^{79} & u_{19}^{78} & 0 \\ u_{27}^{89} & u_{28}^{79} & u_{29}^{78} & 0 \\ u_{37}^{89} & u_{38}^{79} & u_{39}^{78} & 0 \\ u_{47}^{89} & u_{48}^{79} & u_{49}^{78} & 0 \end{bmatrix} \begin{bmatrix} \tilde{\omega}_7 \\ \tilde{\omega}_8 \\ \tilde{\omega}_9 \\ 0 \end{bmatrix} \tag{7.13}$$

Thus, the task of defining transmission ratios can be solved as a task of kinematic analysis of planar linkage mechanism with one degree of freedom. All transmission ratios are function of input angles φ_7 , φ_8 and φ_9 .

Using equations (7.9) and (7.13) we can get equation of kinetic energy of mechanical system as;

$$2T = I_{77}\omega_7^2 + I_{88}\omega_8^2 + I_{99}\omega_9^2 + 2I_{78}\omega_7\omega_8 + 2I_{79}\omega_7\omega_9 + 2I_{89}\omega_8\omega_9 \tag{7.14}$$

where I_{77} , I_{88} , I_{99} , I_{78} , I_{79} and I_{89} are called inertial coefficients.

$$\begin{aligned}
I_{77} &= I_7 + I_1(u_{17}^{89})^2 + I_2(u_{27}^{89})^2 + I_3(u_{37}^{89})^2 + I_4(u_{47}^{89})^2 \\
I_{88} &= I_8 + I_1(u_{18}^{79})^2 + I_2(u_{28}^{79})^2 + I_3(u_{38}^{79})^2 + I_4(u_{48}^{79})^2 \\
I_{99} &= I_9 + I_1(u_{19}^{78})^2 + I_2(u_{29}^{78})^2 + I_3(u_{39}^{78})^2 + I_4(u_{49}^{78})^2 \\
I_{78} &= I_1 u_{17}^{89} u_{18}^{79} + I_2 u_{27}^{89} u_{28}^{79} + I_3 u_{37}^{89} u_{38}^{79} + I_4 u_{47}^{89} u_{48}^{79} \\
I_{79} &= I_1 u_{17}^{89} u_{19}^{78} + I_2 u_{27}^{89} u_{29}^{78} + I_3 u_{37}^{89} u_{39}^{78} + I_4 u_{47}^{89} u_{49}^{78} \\
I_{89} &= I_1 u_{18}^{79} u_{19}^{78} + I_2 u_{28}^{79} u_{29}^{78} + I_3 u_{38}^{79} u_{39}^{78} + I_4 u_{48}^{79} u_{49}^{78}
\end{aligned}$$

Derivative equation of kinetic energy (7.14) for input angles ϕ_7 , ϕ_8 and ϕ_9 gives;

$$\begin{bmatrix} \partial T / \partial \phi_7 \\ \partial T / \partial \phi_8 \\ \partial T / \partial \phi_9 \end{bmatrix} = \begin{bmatrix} \frac{1}{2} \frac{\partial I_{77}}{\partial \phi_7} & \frac{1}{2} \frac{\partial I_{88}}{\partial \phi_7} & \frac{1}{2} \frac{\partial I_{99}}{\partial \phi_7} & \frac{\partial I_{78}}{\partial \phi_7} & \frac{\partial I_{79}}{\partial \phi_7} & \frac{\partial I_{89}}{\partial \phi_7} \\ \frac{1}{2} \frac{\partial I_{77}}{\partial \phi_8} & \frac{1}{2} \frac{\partial I_{88}}{\partial \phi_8} & \frac{1}{2} \frac{\partial I_{99}}{\partial \phi_8} & \frac{\partial I_{78}}{\partial \phi_8} & \frac{\partial I_{79}}{\partial \phi_8} & \frac{\partial I_{89}}{\partial \phi_8} \\ \frac{1}{2} \frac{\partial I_{77}}{\partial \phi_9} & \frac{1}{2} \frac{\partial I_{88}}{\partial \phi_9} & \frac{1}{2} \frac{\partial I_{99}}{\partial \phi_9} & \frac{\partial I_{78}}{\partial \phi_9} & \frac{\partial I_{79}}{\partial \phi_9} & \frac{\partial I_{89}}{\partial \phi_9} \end{bmatrix} \begin{bmatrix} \omega_7 \omega_7 \\ \omega_8 \omega_8 \\ \omega_9 \omega_9 \\ \omega_7 \omega_8 \\ \omega_7 \omega_9 \\ \omega_8 \omega_9 \end{bmatrix} \quad (7.15)$$

Inertial coefficients depends on transmission ratios $(u_{17}^{89}, u_{27}^{89}, u_{37}^{89}, u_{47}^{89})$, $(u_{18}^{79}, u_{28}^{79}, u_{38}^{79}, u_{48}^{79})$ and $(u_{19}^{78}, u_{29}^{78}, u_{39}^{78}, u_{49}^{78})$ which also depends on input angles ϕ_7 , ϕ_8 and ϕ_9 . Partial derivation of internal coefficients can be introduced in matrix form as follows

$$\mathbf{A} = \mathbf{B} \times \mathbf{u}$$

$$\mathbf{A} = \begin{bmatrix} \partial I_{77} / \partial \phi_7 \\ \partial I_{77} / \partial \phi_8 \\ \partial I_{77} / \partial \phi_9 \\ \partial I_{88} / \partial \phi_7 \\ \partial I_{88} / \partial \phi_8 \\ \partial I_{88} / \partial \phi_9 \\ \partial I_{99} / \partial \phi_7 \\ \partial I_{99} / \partial \phi_8 \\ \partial I_{99} / \partial \phi_9 \\ \partial I_{78} / \partial \phi_7 \\ \partial I_{78} / \partial \phi_8 \\ \partial I_{78} / \partial \phi_9 \\ \partial I_{79} / \partial \phi_7 \\ \partial I_{79} / \partial \phi_8 \\ \partial I_{79} / \partial \phi_9 \\ \partial I_{89} / \partial \phi_7 \\ \partial I_{89} / \partial \phi_8 \\ \partial I_{89} / \partial \phi_9 \end{bmatrix} \quad \mathbf{u} = \begin{bmatrix} I_1 u_{17}^{89} \\ I_2 u_{27}^{89} \\ I_3 u_{37}^{89} \\ I_4 u_{47}^{89} \\ I_1 u_{18}^{79} \\ I_2 u_{28}^{79} \\ I_3 u_{38}^{79} \\ I_4 u_{48}^{79} \\ I_1 u_{19}^{78} \\ I_2 u_{29}^{78} \\ I_3 u_{39}^{78} \\ I_4 u_{49}^{78} \end{bmatrix} \quad (7.16)$$

Derivative expression of kinetic energy (7.19) for input velocities ω_7 , ω_8 and ω_9 yields;

$$\begin{bmatrix} \frac{\partial T}{\partial \omega_7} \\ \frac{\partial T}{\partial \omega_8} \\ \frac{\partial T}{\partial \omega_9} \end{bmatrix} = \begin{bmatrix} I_{77} & I_{78} & I_{79} \\ I_{78} & I_{88} & I_{89} \\ I_{79} & I_{89} & I_{99} \end{bmatrix} \begin{bmatrix} \omega_7 \\ \omega_8 \\ \omega_9 \end{bmatrix} \quad (7.17)$$

Time derivative of equation (7.17) gives;

$$\begin{bmatrix} \frac{d}{dt} \frac{\partial T}{\partial \omega_7} \\ \frac{d}{dt} \frac{\partial T}{\partial \omega_8} \\ \frac{d}{dt} \frac{\partial T}{\partial \omega_9} \end{bmatrix} = \begin{bmatrix} I_{77} & I_{78} & I_{79} \\ I_{78} & I_{88} & I_{89} \\ I_{79} & I_{89} & I_{99} \end{bmatrix} \begin{bmatrix} \varepsilon_7 \\ \varepsilon_8 \\ \varepsilon_9 \end{bmatrix} + \begin{bmatrix} \frac{dI_{77}}{dt} & \frac{dI_{78}}{dt} & \frac{dI_{79}}{dt} \\ \frac{dI_{78}}{dt} & \frac{dI_{88}}{dt} & \frac{dI_{89}}{dt} \\ \frac{dI_{79}}{dt} & \frac{dI_{89}}{dt} & \frac{dI_{99}}{dt} \end{bmatrix} \begin{bmatrix} \omega_7 \\ \omega_8 \\ \omega_9 \end{bmatrix} \quad (7.18)$$

Derivation of inertia coefficients (7.14) (inertia coefficients are function of input angles φ_7 , φ_8 and φ_9) gives;

$$\begin{bmatrix} \frac{dI_{77}}{dt} \\ \frac{dI_{88}}{dt} \\ \frac{dI_{99}}{dt} \\ \frac{dI_{78}}{dt} \\ \frac{dI_{79}}{dt} \\ \frac{dI_{89}}{dt} \end{bmatrix} = \begin{bmatrix} \frac{\partial I_{77}}{\partial \varphi_7} & \frac{\partial I_{77}}{\partial \varphi_8} & \frac{\partial I_{77}}{\partial \varphi_9} & 0 & 0 & 0 \\ \frac{\partial I_{88}}{\partial \varphi_7} & \frac{\partial I_{88}}{\partial \varphi_8} & \frac{\partial I_{88}}{\partial \varphi_9} & 0 & 0 & 0 \\ \frac{\partial I_{99}}{\partial \varphi_7} & \frac{\partial I_{99}}{\partial \varphi_8} & \frac{\partial I_{99}}{\partial \varphi_9} & 0 & 0 & 0 \\ \frac{\partial I_{78}}{\partial \varphi_7} & \frac{\partial I_{78}}{\partial \varphi_8} & \frac{\partial I_{78}}{\partial \varphi_9} & 0 & 0 & 0 \\ \frac{\partial I_{79}}{\partial \varphi_7} & \frac{\partial I_{79}}{\partial \varphi_8} & \frac{\partial I_{79}}{\partial \varphi_9} & 0 & 0 & 0 \\ \frac{\partial I_{89}}{\partial \varphi_7} & \frac{\partial I_{89}}{\partial \varphi_8} & \frac{\partial I_{89}}{\partial \varphi_9} & 0 & 0 & 0 \end{bmatrix} \begin{bmatrix} \omega_7 \\ \omega_8 \\ \omega_9 \\ 0 \\ 0 \\ 0 \end{bmatrix} \quad (7.19)$$

Using equations (7.9), (7.15), (7.18) and (7.19), we can get Lagrange motion equation for mechanical system with three degrees of freedom in the following form;

$$\begin{aligned} M_{e1} = & I_{77}\varepsilon_7 + I_{78}\varepsilon_8 + I_{79}\varepsilon_9 + \frac{1}{2} \frac{\partial I_{77}}{\partial \varphi_7} \omega_7^2 + \left(\frac{\partial I_{78}}{\partial \varphi_8} - \frac{1}{2} \frac{\partial I_{88}}{\partial \varphi_7} \right) \omega_8^2 + \left(\frac{\partial I_{79}}{\partial \varphi_9} - \frac{1}{2} \frac{\partial I_{99}}{\partial \varphi_7} \right) \omega_9^2 \\ & + \frac{\partial I_{77}}{\partial \varphi_8} \omega_7 \omega_8 + \frac{\partial I_{77}}{\partial \varphi_9} \omega_7 \omega_9 + \left(\frac{\partial I_{78}}{\partial \varphi_9} + \frac{\partial I_{79}}{\partial \varphi_8} - \frac{\partial I_{89}}{\partial \varphi_7} \right) \omega_8 \omega_9 \end{aligned} \quad (7.20)$$

$$\begin{aligned} M_{e2} = & I_{78}\varepsilon_7 + I_{88}\varepsilon_8 + I_{89}\varepsilon_9 + \left(\frac{\partial I_{78}}{\partial \varphi_7} - \frac{1}{2} \frac{\partial I_{77}}{\partial \varphi_8} \right) \omega_7^2 + \frac{1}{2} \frac{\partial I_{88}}{\partial \varphi_8} \omega_8^2 + \left(\frac{\partial I_{89}}{\partial \varphi_9} - \frac{1}{2} \frac{\partial I_{99}}{\partial \varphi_8} \right) \omega_9^2 + \frac{\partial I_{88}}{\partial \varphi_7} \omega_7 \omega_8 \\ & + \left(\frac{\partial I_{78}}{\partial \varphi_9} + \frac{\partial I_{89}}{\partial \varphi_7} - \frac{\partial I_{79}}{\partial \varphi_8} \right) \omega_7 \omega_9 + \frac{\partial I_{88}}{\partial \varphi_9} \omega_8 \omega_9 \end{aligned} \quad (7.21)$$

$$\begin{aligned} M_{e3} = & I_{79}\varepsilon_7 + I_{89}\varepsilon_8 + I_{99}\varepsilon_9 + \left(\frac{\partial I_{79}}{\partial \varphi_7} - \frac{1}{2} \frac{\partial I_{77}}{\partial \varphi_9} \right) \omega_7^2 + \left(\frac{\partial I_{89}}{\partial \varphi_8} - \frac{1}{2} \frac{\partial I_{88}}{\partial \varphi_9} \right) \omega_8^2 + \frac{1}{2} \frac{\partial I_{99}}{\partial \varphi_9} \omega_9^2 \\ & + \left(\frac{\partial I_{89}}{\partial \varphi_7} + \frac{\partial I_{79}}{\partial \varphi_8} - \frac{\partial I_{78}}{\partial \varphi_9} \right) \omega_7 \omega_9 + \frac{\partial I_{99}}{\partial \varphi_7} \omega_7 \omega_9 + \frac{\partial I_{99}}{\partial \varphi_8} \omega_8 \omega_9 \end{aligned} \quad (7.22)$$

Equation (7.20), (7.21) and (7.22) describe equations of motion for the left side of LBS rover suspension system. By applying same procedure to the other side of the rover, we get six Lagrange motion equations for a mobile robot suspension mechanism with six degrees of freedom.

Chapter 8

COMPUTER SIMULATION

8.1 Rover Drive on Test Course

Computer modelling and simulation is powerful tool for designers. Although the suspension mechanism calculated by mathematically and geometrically, visual test with modern computer programs is another important phase of a suspension research.

Main performance criteria of a rover suspension is its force distribution on the ground. To measure the approximate behaviour of linear bogie, a computer model has been constructed and assembled. On different test courses, experimental LBS rover driven and measured its reaction forces and positions. During planar motion tests, only one side of the mechanism simulated to decrease the solution period.

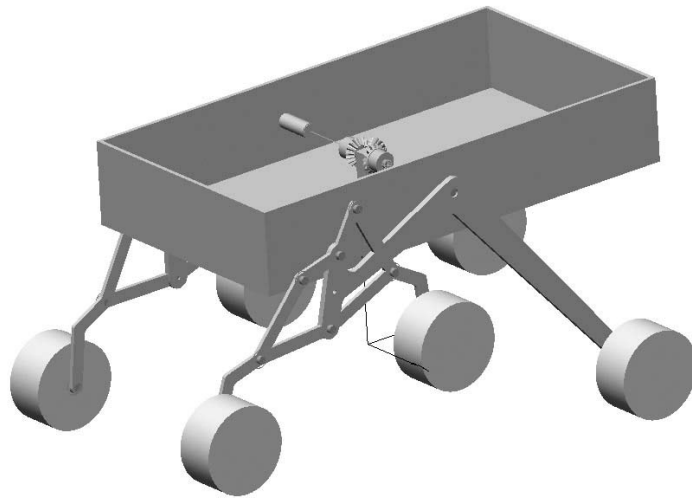


Figure 8-1: Rover computer model for simulation

8.1.1 Hill Climbing

First test course is a convex shaped hollow. Maximum depth of course is approximately 500 millimeters. Total travelling time is 2 seconds. Actuators are rotating at constant velocity of 2π rad/sec during simulation. The rover's weight is assumed as 200 kgs.



Figure 8-2: Test course

Reaction forces at front, middle and rear wheel, which is an indicator of traction force on rough terrain, is given below.

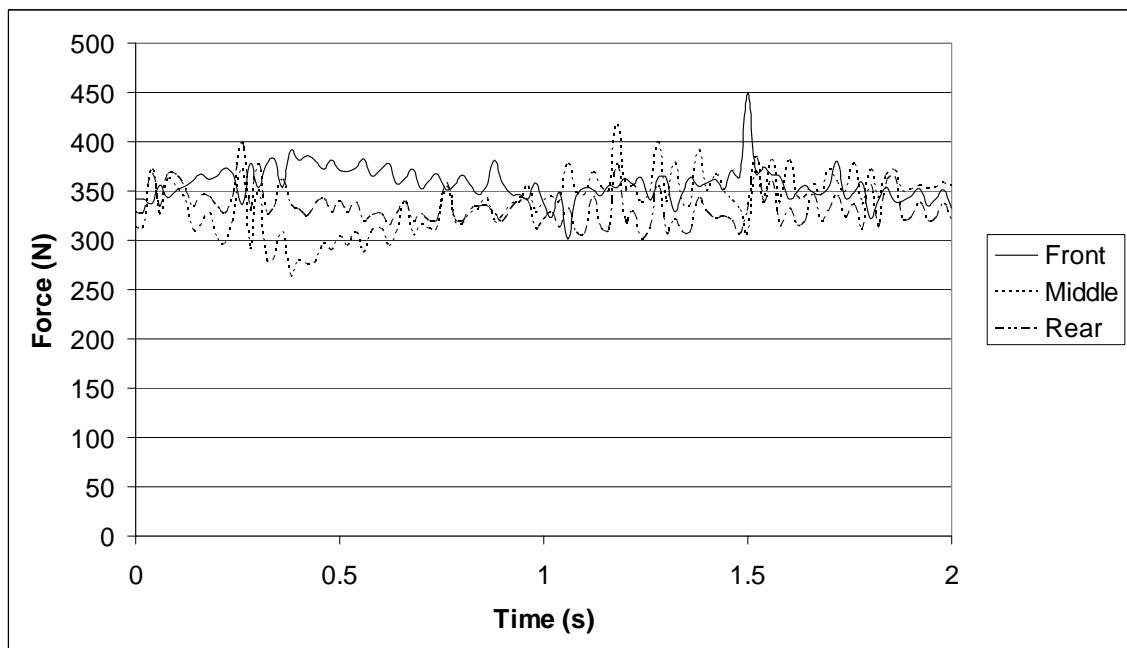


Figure 8-3: Wheel reaction forces on test course

It can be seen on figure 8-3; reaction forces have close values to each other. Small waves are result of rough terrain where wheels softly bounce while passing over obstacles. Constant wheel velocities are also another cause of these small deviations.

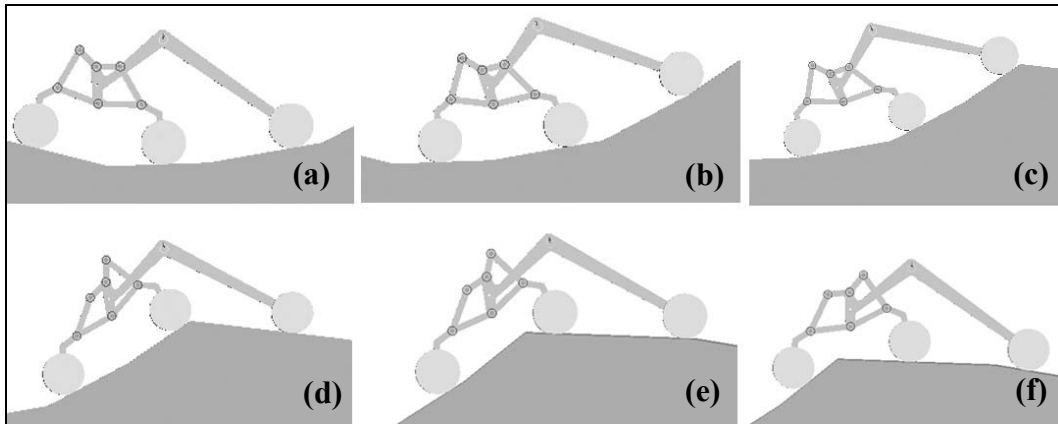


Figure 8-4: Course with small hill

8.1.2 Step Climbing

Another challenging terrain type for mobile robots is step climbing. For indoor usage, stairs are the most significant obstacles. This vertical motion also needs high surface friction coefficient between wheel and ground.

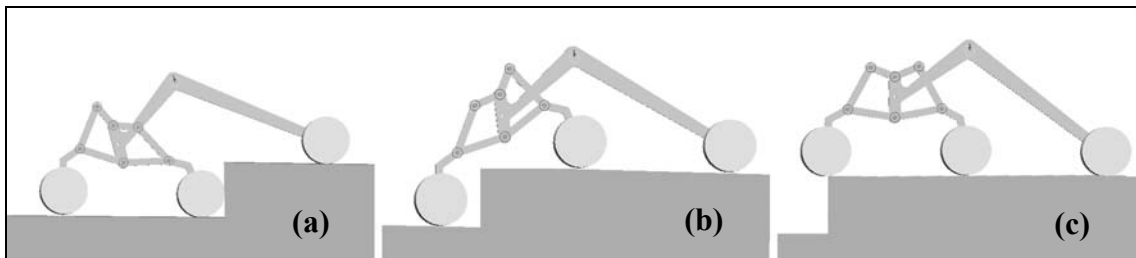


Figure 8-5: Step climbing performance of LBS

In computer simulations, LBS has climbed approximately 1.5 wheel diameter of step obstacle. Linear motion has a natural advantage during vertical climbing. During this motion, reaction force, which acts from obstacle to trajectory, is perpendicular to trajectory of the wheel. By the advantage of this motion dangerous moment on bogie prevented with mechanism.

8.2 Evaluation of Test Results

After different field and obstacle simulations, LBS design demonstrates a similar obstacle capacity with *rocker-bogie* suspension. Advantage of the linear suspension is its more reliable structure with linear motion. This feature also can be a transition from quasi-static operation to fast-speed operation of planetary rovers.

Since climbing operations need high surface friction, a vehicle which can climb an obstacle more than 2 wheel diameters should have an active climbing system. Passive suspension mechanisms capacity limit depends on wheel diameter where the limit narrowed by overall size of the robot.

Chapter 9

CONCLUSION

In this thesis study, rover suspension mechanisms have been discussed. Linear motion mechanism of Chebyshev has been improved and applied for a Mars rover suspension mechanism. Results of the simulations and position analysis show that linear motion bogie has good performance during field operations. On the other hand, different designs should be discussed to improve the capacity of suspension.

This research also shows that it is possible to construct useful mechanisms by arranging classical four-bar mechanisms. These design possibilities can be discussed with new structural synthesis formula, which has been introduced and applied on rover suspension design.

Future studies may continue to discuss dynamic behaviour of the suspension mechanism. Anyone can see that planetary exploration will be the future robotics topic with unusual mobility and high stamina robots.

The purpose of this study is to put another stone on the pyramid of scientific knowledge. Although the art of mechanism design seems like it has lost its popularity due to the powerful control algorithms, there is no doubt that future robotics study will continue to search for new mechanisms.

REFERENCES

- [1] B.Vilcox, T.Nguyen, Sojourner on Mars and Lessons Learned for Future Planetary Rovers, ICES, 1997
- [2] National Aeronautics and Space Administration (NASA) Mars Exploration Rover Landings Press Kit (January 2004)
- [3] G.Dudek, M.Jenkin *Computational Principles of Mobile Robotics* (Cambridge – United Kingdom – 2000)
- [4] P.E.Sandin, *Robot Mechanisms and Mechanical Devices Illustrated* (McGraw Hill – New York – 2003)
- [5] J.C.Dixon, *Tires, Suspension and Handling* Second Edition, Society of Automotive Engineers (Arnold – London – 1996)
- [6] E.Söylemez, *Mechanisms*, Middle East Technical University, Publication Number: 64 (Ankara - Turkey, 1999)
- [7] K.Hain, *Applied Kinematics* Second Edition (McGraw Hill - New York - 1967)
- [8] N.I.Levitski, *Theory of Mechanism and Machines* (Moscow-1990) in Russian
- [9] I.I.Artobolevski, N.I.Levitski, S.A.Cherrudinov. Synthesis of Plane Mechanisms (Fizmathgiz – Moscow – 1959) p.687, in Russian
- [10] National Aeronautics and Space Administration (NASA) Mars Exploration Rovers Web Site <http://marsrovers.nasa.gov>
- [11] P.Fiorini, Ground Mobility Systems for Planetary Exploration Proceedings of the 2000 IEEE - ICRA (April 2000) p 908-913

- [12] P.L.Chebyshev, *To Parallelograms* (Academy of Science, Moscow - Russia 1955 Originally 1869), in Russian
- [13] M.Faires, R.M.Keawn, *Mechanism*, Fifth Edition (McGraw Hill – New York – 1960)
- [14] R.Siegwart, P.Lamon, T.Estier, M.Lauria, R.Piguet, Innovative design for wheeled locomotion in rough terrain, *Robotics and Autonomous Systems* 40 (2002) 151-162
- [15] R.G.Bonitz, T.T.Nguyen, W.S.Kim, The Mars Surveyor '01 Rover and Robotic Arm, *IEEE*, 0-7803-5846-5, 2000
- [16] J.A.Jones, J.J.Wu, “Inflatable Rovers for Planetary Applications”, Proceedings of the SPIE International Symposium on Intelligent Systems and Advanced Manufacturing September 19-22, Boston, MA, 1999
- [17] L.Tsai, *Robot Analysis: The Mechanics of Serial and Parallel Manipulators* (John – Wiley & Sons -United States - 1999)
- [18] M.Z.Kolovsky, A.N.Evgrafov, Y.A.Semenov *Advanced Theory of Mechanisms and Machines* (Springer, Berlin – Germany – 2000)
- [19] D.B.Bickler “Articulated Suspension System” US 4,840,394 (United States Patent – June 20, 1989)
- [20] M.Grübler, Allgemeine eigenschaften für swangläufigen ebenen kinemischen ketten, part I, (29) (1883) 167-200
- [21] M.Grübler, Allgemeine eigenschaften für swangläufigen ebenen kinemischen ketten, part II, (64) (1885) 179-229
- [22] F.Freudenstein, R.Alizade, On the degree of freedom of mechanisms with variable general constraint, IV World IFToMM Congress, England (1975) 51-56

- [23] R.Alizade, On the DOF of kinematic chains, Az. Pol. Inst. Baku (1988)
3–14, in Russian
- [24] Ç.Bayram, Kinematic and dynamic analysis of spatial six degree of freedom parallel structure manipulator Master of Science thesis İzmir Inst. of Tech. (2003)
- [25] R.Alizade, Ç.Bayram, Structural synthesis of parallel manipulators Mechanism and Machine Theory (in press - 2004)
- [26] D.S.Apostolopoulos, Analytical configuration of wheeled robotic locomotion, PhD Thesis Carnegie Mellon University, CMU-RI-TR-01-08 (2001)
- [27] R.Volpe, I.Balaram, T.Ohm, R.Ivlev, Rocky 7: A next generation Mars rover prototype, Journal of Advanced Robotics., 11(4), December 1997
- [28] K.Iagnemma, A.Rzepniewski, S.Dubowsky, P.Pirjanian, T.Huntsberger, and P.Schenker, Mobile robot kinematic reconfigurability for rough-terrain, Proceedings of the SPIE International Symposium on Intelligent Systems and Advanced Manufacturing, August 2000
- [29] National Aeronautics and Space Administration (NASA) Jet Propulsion Laboratory Nanorover web site <http://robotics.jpl.nasa.gov/tasks/nrover/>
- [30] H.Hacot, S.Dubowsky, P.Bidaud, Analysis and simulation of a rocker-bogie exploration rover, Proceedings of the Twelfth CISM-IFT.MM Symposium on Theory and Practice of Robots and Manipulators, Paris, France, July 6-9, 1998.
- [31] H.Hacot, "Analysis and Traction Control of a Rocker-Bogie Planetary Rover," Master of Science Thesis, Department of Mechanical Engineering, MIT, 1998
- [32] Y.Chung, J.Choo, J.Lee, SenSation: A new 2 DOF parallel mechanism for a haptic device, 1st Russian Korean International Symposium on Applied Mechanics, pp.191-199., Oct. 2-4, 2001, Russia.

- [33] M.Thianwiboon, V.Sangveraphunsiri, R.Chancharoen, Rocker-bogie suspension performance, The eleventh International Pacific Conference in Automotive Engineering (IPC-11). November 6-9, 2001. Shanghai China.
- [34] S.Sasaki, T.Kubota, T.Okada, Y.Kuroda, Y.Kunij, E.Shibamura, N.Akiyama, M.Ohtake, M.Ichikawa, M.Higa, N.Hirata, T.Sugihara, J.Haruyama, H.Otake, N.Yoshioka, J.Terazono, M.Yamada, Y.Yamaguchi, S.Koadama and Rover group in Japan, Scientific exploration of lunar surface using a rover in Japanese future Lunar mission, *Adv. Space Res.* Vol.30 No.8 pp. 1921-1926 (2002)
- [35] D.Miller, T.Lee, High-speed traversal of rough terrain using a rocker-bogie mobility system, *Proceedings of Robotics 2002: The 5th International Conference and Exposition on Robotics for Challenging Situations and Environments*, Albuquerque, New Mexico, March 2002.
- [36] S.Farritor, H.Hacot, S.Dubovsky, Physics-based planning for planetary exploration, *Proceedings of the 1998 IEEE International Conference on Robotics and Automation*, Leuven, Belgium, Vol. 1, pp. 278-283, May 1998
- [37] S.Farritor, H.Hacot, S.Dubowsky, Physics-based planning for planetary exploration, *IEEE International Conference on Robotic and Automation*, 1998
- [38] D.P.Miller, M.J.Roman, A.Winterholler, T.S.Hunt, Experiments with a Long Range planetary rover, *Proceedings of the The 7th International Symposium on Artificial Intelligence, Robotics and Automation in Space*, Nara, Japan, May 2003
- [39] S.V.Sreenivasan, P.Nanua, Kinematic geometry of wheeled vehicle systems, *Journal of Mechanical Design*, Vol.121, p.50-56, March 1999
- [40] S.V.Sreenivasan, K. J. Displacement analysis of an actively articulated wheeled vehicle configuration with extensions to motion planning on uneven terrain, *Journal of Mechanical Design* Vol. 118, p. 312-317, June 1996

- [41] A.Ellery, *An introduction to space robotics*, (Springer – London -2000)
- [42] R.Alizade, Kinematic analysis and synthesis of spatial linkage mechanisms by module method, Dissertation for the degree of Doctor of Science, Baku, 1992
- [43] R.Alizade, Physical substance and geometrical interpretation of variable constraint parameters of universal structural formula, Azerbaijan Technical University, (1991) 3-12, in Russian
- [44] R.Alizade, Sh.Aliyev, A.Temirov, I.Mamedov, Analysis of variable constraint parameters of universal structural formula, Azerbaijan Technical University, 6(1) (1997) p162-166, in Russian
- [45] R.Alizade, E.T.Hajiev, G.N.Sandor, Type synthesis of spatial mechanisms on the basis of spatial single loop structural groups, Mechanism and Machine Theory, 20(2) (1985) p. 95-101
- [46] R.Alizade, Investigation of linkage mechanisms with lower pairs from point of view of its structure and classification, Azerb. Poly. Inst, Baku (1988) p. 111-127, in Russian
- [47] P.Putz, Space Robotics in Europe: A survey, Robotics and Autonomous Systems 23 (1998) p. 3-16
- [48] P.S.Schenker, T.L.Huntsberger, P.Pirjanian, E.T.Baumgartner, and E.Tunstel, Planetary rover developments supporting Mars exploration, sample return and future human-robotic colonization, Autonomous Robots, Vol. 14, pp. 103-126, 2003.
- [49] L.L.Howell, *Compliant Mechanisms*, p.277 (Wiley – New York - 2001)
- [50] S.Molian, *Mechanism Design The practical kinematics and dynamics of machinery*, Second Edition p.54 (Elsevier – London – 1997)

Appendix A

DIMENSIONS OF SUSPENSION MECHANISM AND ROVER

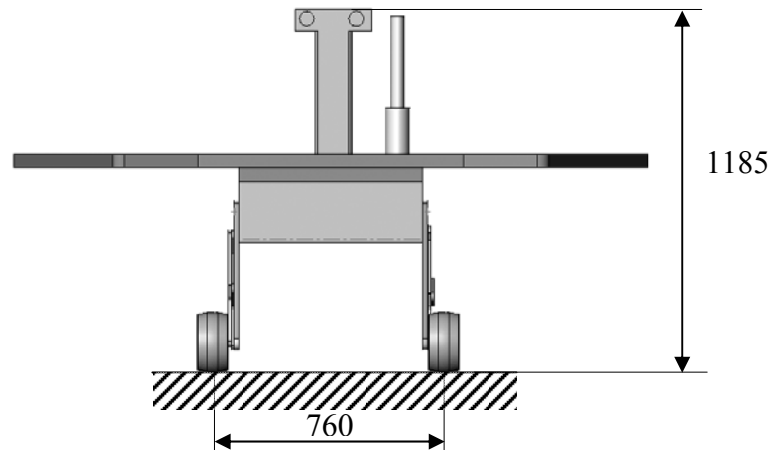


Figure A1.1: General dimensions of the rover (Front View)

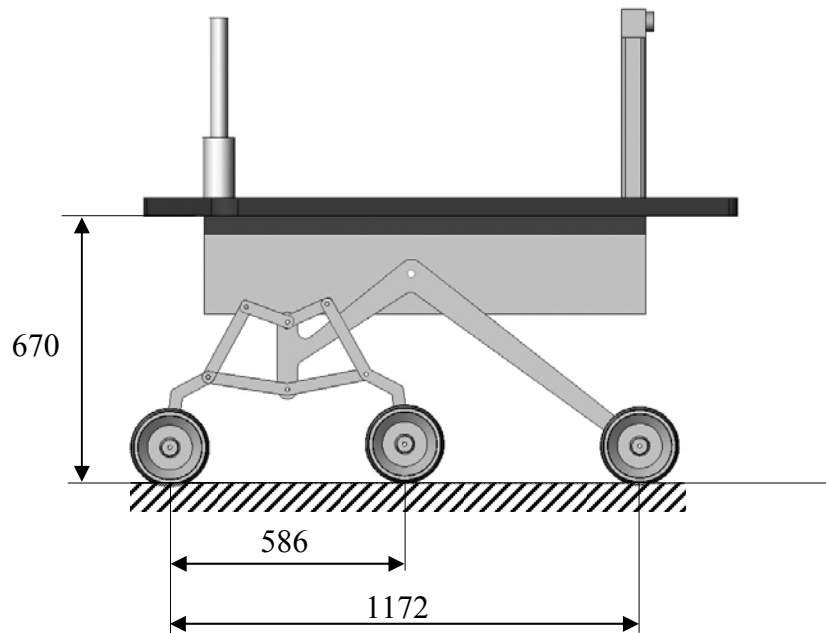


Figure A1.2: General dimensions of the rover (Side View)

Note: All dimensions are given in millimeters

Appendix B

CONSTRAINT FUNCTION SOLUTION

In solution of four-bar mechanisms,

$$A(\theta)\cos\psi + B(\theta)\sin\psi = C(\theta) \quad (\text{A 2.1})$$

We can solve this equation by two methods.

For trigonometric solution we divide both sides by $\sqrt{A^2 + B^2}$. That yields;

$$\cos\delta = \frac{A}{\sqrt{A^2 + B^2}} \quad \text{and} \quad \sin\delta = \frac{B}{\sqrt{A^2 + B^2}} \quad (\text{A 2.2})$$

If we divide and arrange these two equations;

$$\delta = \arctan\left(\frac{B}{A}\right) \quad (\text{A 2.3})$$

If we put this term into (A 2.1)

$$\cos\delta\cos\psi + \sin\delta\sin\psi = \cos(\psi - \delta) \quad (\text{A 2.4})$$

This equation also another cosine of angle. Let we call this angle τ ;

$$\cos\tau = \frac{C}{\sqrt{A^2 + B^2}} \quad (\text{A 2.5})$$

Because of cosine function has negative and positive term, $\delta+\tau$ and $\delta-\tau$ are solutions.

$$\psi = \delta \pm \tau \quad (\text{A 2.6})$$

$$\psi = \arctan\left(\frac{B}{A}\right) \pm \arccos\left(\frac{C}{\sqrt{A^2 + B^2}}\right) \quad (\text{A 2.7})$$

The solution exists only if $-1 \leq \cos \tau \leq 1$. So that $A^2 + B^2 - C \geq 0$

The second solution method is tan-half-angle technique. In equation (A 2.1) we can transform sine cosine terms with;

$$\cos \psi = \frac{1-u^2}{1+u^2}, \quad \sin \psi = \frac{2u}{1+u^2}, \quad \tan\left(\frac{\psi}{2}\right) = u \quad (\text{A 2.8})$$

If we put and arrange them, we can find

$$(C - A)u^2 + 2Bu + (C + A) = 0 \quad (\text{A 2.9})$$

That gives;

$$u = \frac{-B \pm \sqrt{B^2 - (C^2 - A^2)}}{C - A} \quad (\text{A 2.10})$$

and if we put this term into (A 2.8) we get,

$$\psi = 2 \tan^{-1}\left(\frac{-B \pm \sqrt{B^2 - (C^2 - A^2)}}{C - A}\right) \quad (\text{A 2.11})$$

Appendix C

POSITION ANALYSIS WITH MICROSOFT OFFICE EXCEL

Microsoft Excel[®] is a spreadsheet program with number of cells. Cells consist of columns and rows, which can be adapted into two-dimensional components. It is very easy to solve a mechanism if we derive the coupler curve function mathematically.

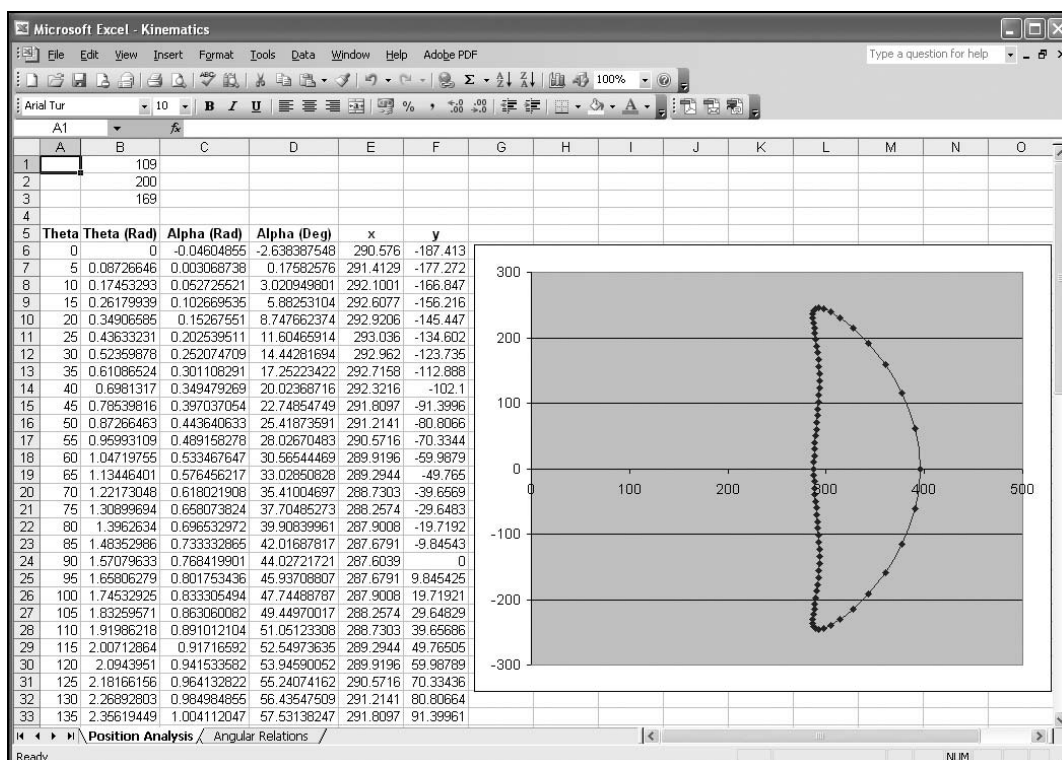


Figure A3.1: Screenshot of Microsoft Excel

The trajectory of the mechanism can be drawn according to one input angle. Other angles were calculated in another sheet from trigonometric relations.

Appendix D

KINEMATIC ANALYSIS WITH VISUAL NASTRAN 4D

MSC Visual Nastran 4D[®] is a kinematic and dynamic simulation program. Mechanism parts are usually modeled with different CAD programs can be easily imported to Visual Nastran. After this procedure, kinematic relations between each body are defined in 3D environment.

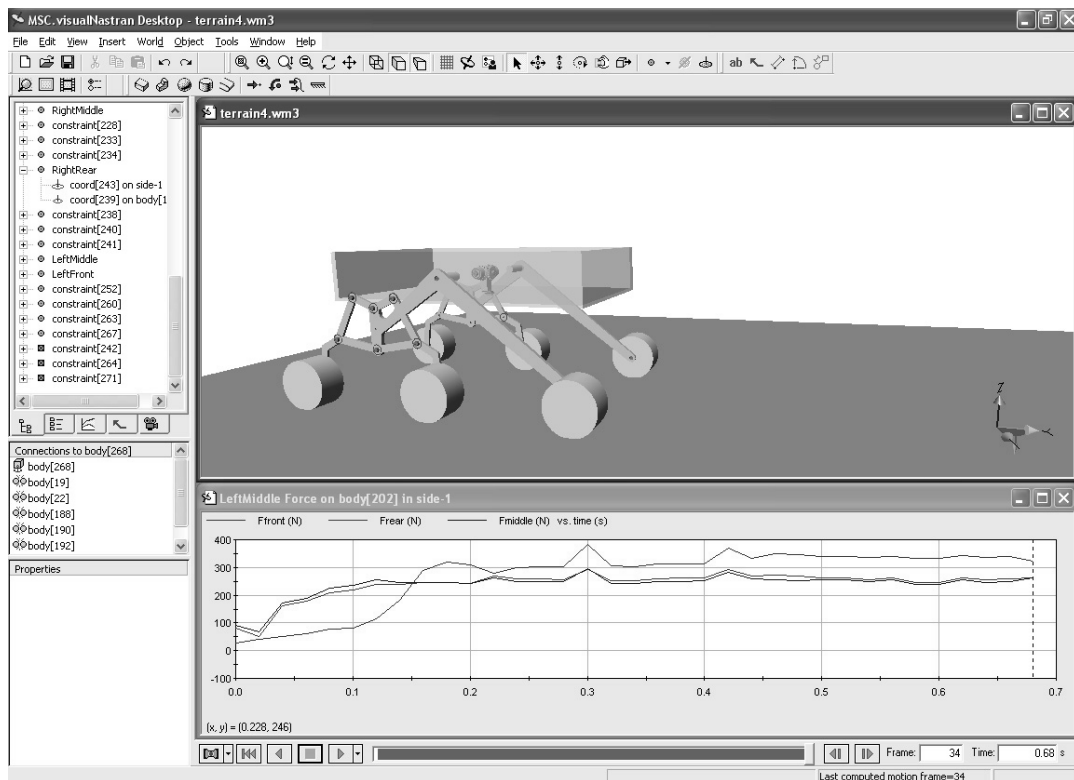


Figure A4.1: Visual Nastran screenshot

Once the model has been constructed, various scenarios can be defined and tested with different files.